4-Cyanopyridine complexes $[MX_2(4\text{-CNpy})_x]_n$ (with X = Cl, Br and x = 1, 2): Crystal structures, thermal properties and a comparison with $[MX_2(3\text{-CNpy})_x]_n$ complexes

Miriam Heine, Lothar Fink, Martin U. Schmidt*

Institute of Inorganic and Analytical Chemistry, Goethe University, Max-von-Laue-Str. 7, 60438 Frankfurt am Main, Germany. E-Mail: heine@chemie.uni-frankfurt.de, fink@chemie.uni-frankfurt.de, m.schmidt@chemie.uni-frankfurt.de; Fax: +49 69798 29235; Tel: +49 69798 29171

Figures

Tables

Experimental details

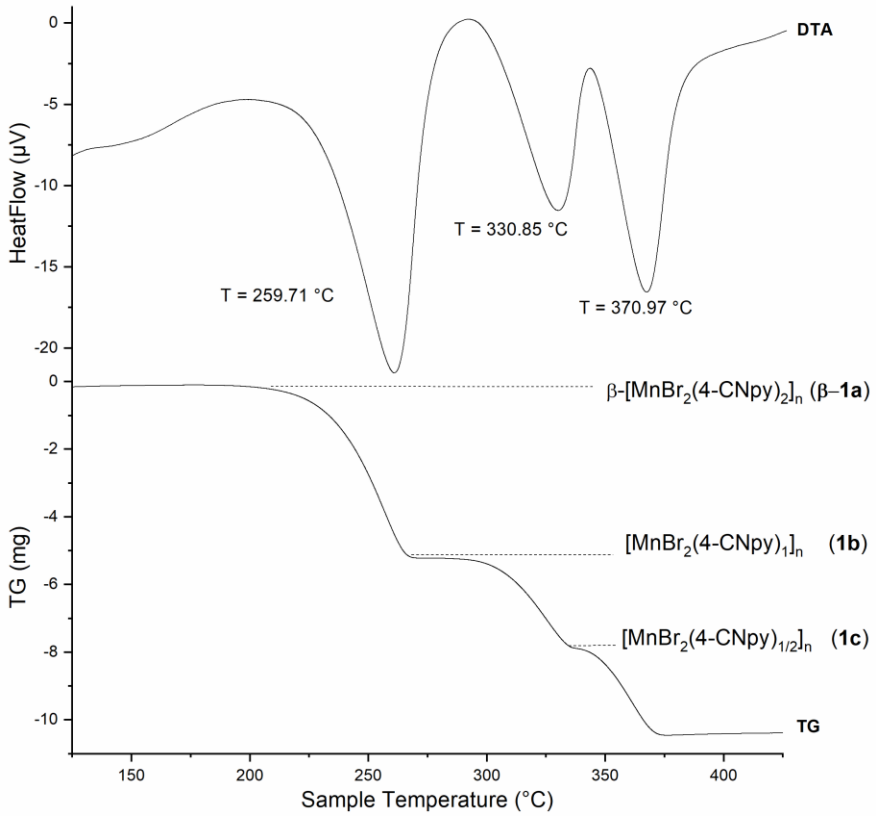

Figure S1. DTA/TG curves of β-$[MnBr_2(4\text{-}CNpy)_2]_n$ (**β-1a**). Heating rate: 5 K/min, Ar atmosphere, Al_2O_3 crucible.

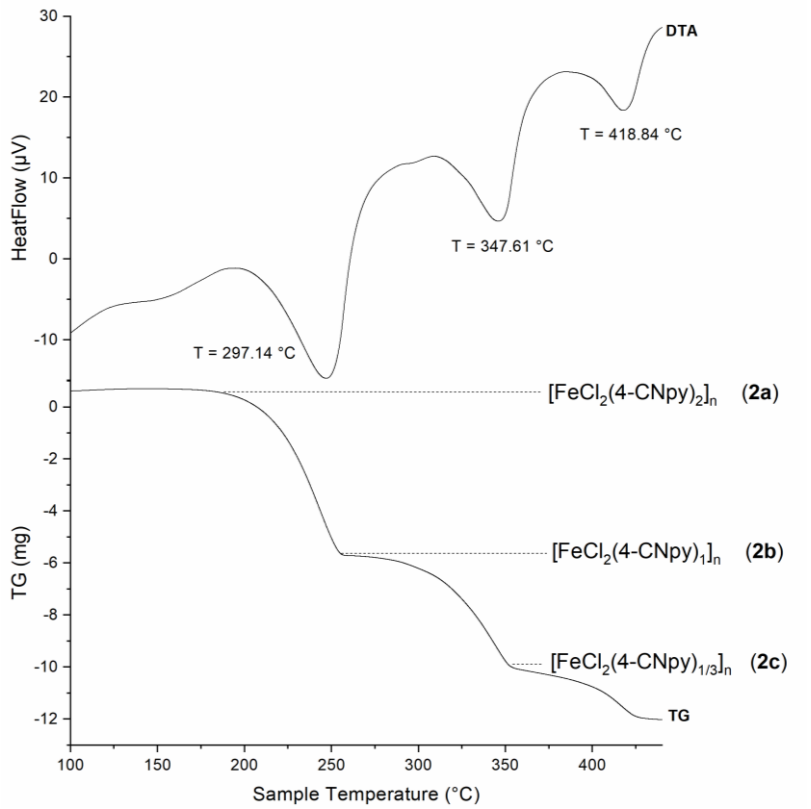

Figure S2. DTA/TG curves of $[FeCl_2(4\text{-}CNpy)_2]_n$ (**2a**). Heating rate: 5 K/min, Ar atmosphere, Al_2O_3 crucible.

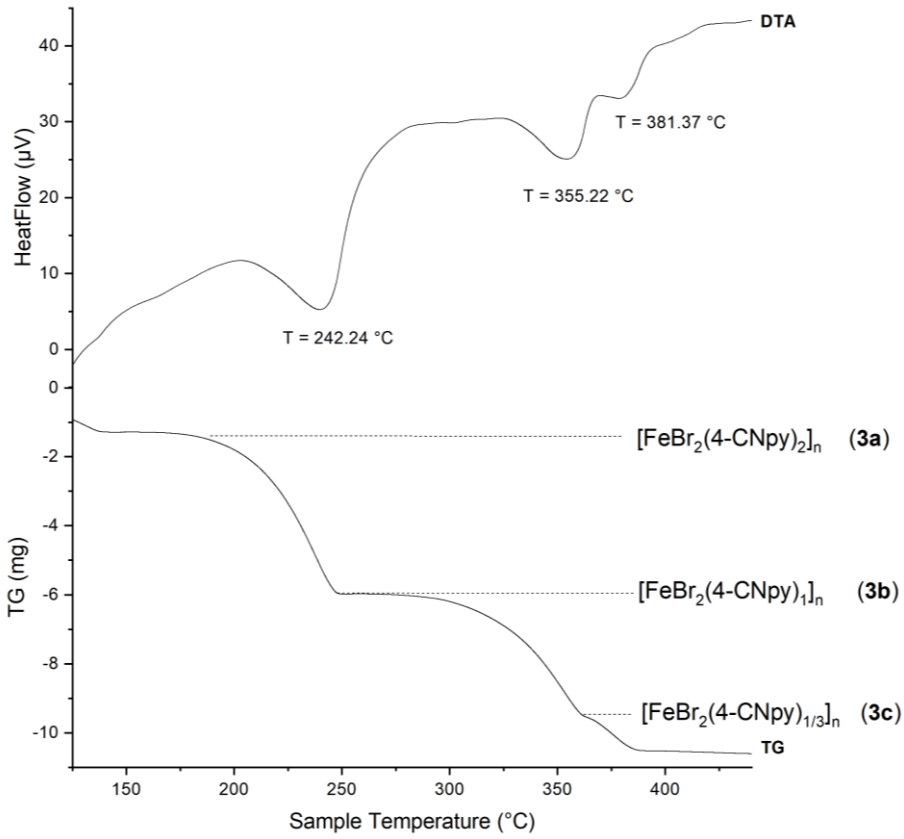

Figure S3. DTA/TG curves of $[FeBr_2(4\text{-}CNpy)_2]_n$ (**3a**). Heating rate: 5 K/min, Ar atmosphere, Al_2O_3 crucible.

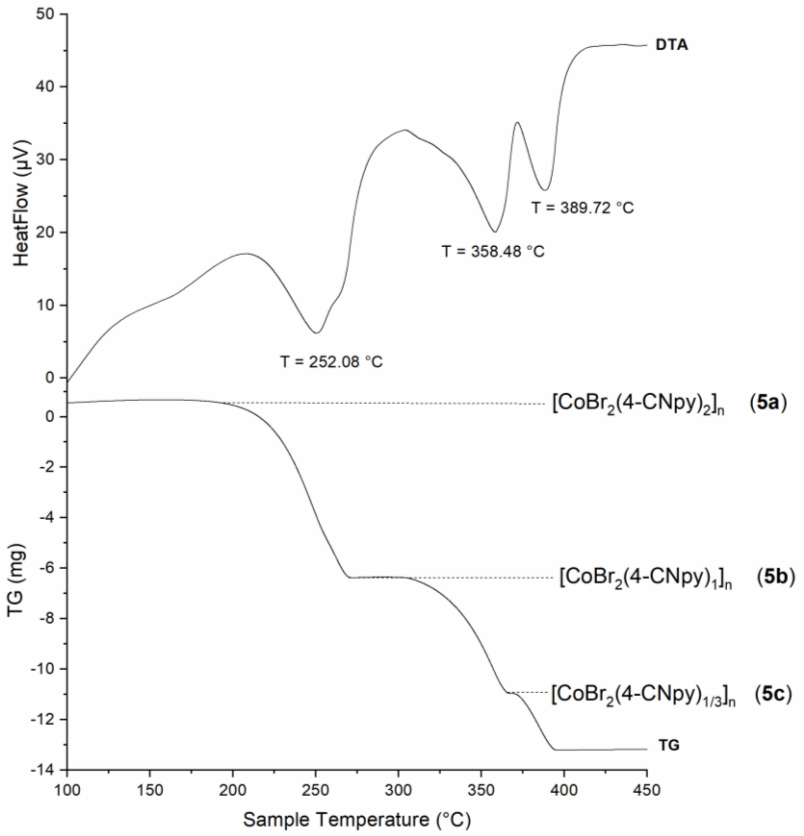

Figure S4. DTA/TG curves of $[CoBr_2(4\text{-}CNpy)_2]_n$ (**5a**). Heating rate: 5 K/min, Ar atmosphere, Al_2O_3 crucible.

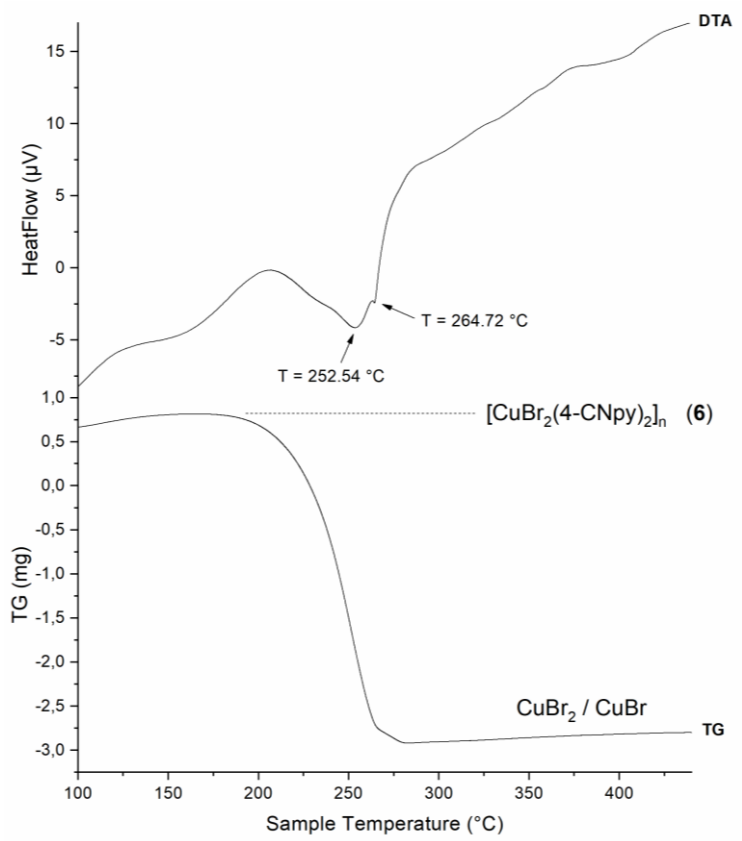

Figure S5. DTA/TG curves of $[CuBr_2(4\text{-}CNpy)_2]_n$ (**6**). Heating rate: 5 K/min, Ar atmosphere, Al_2O_3 crucible.

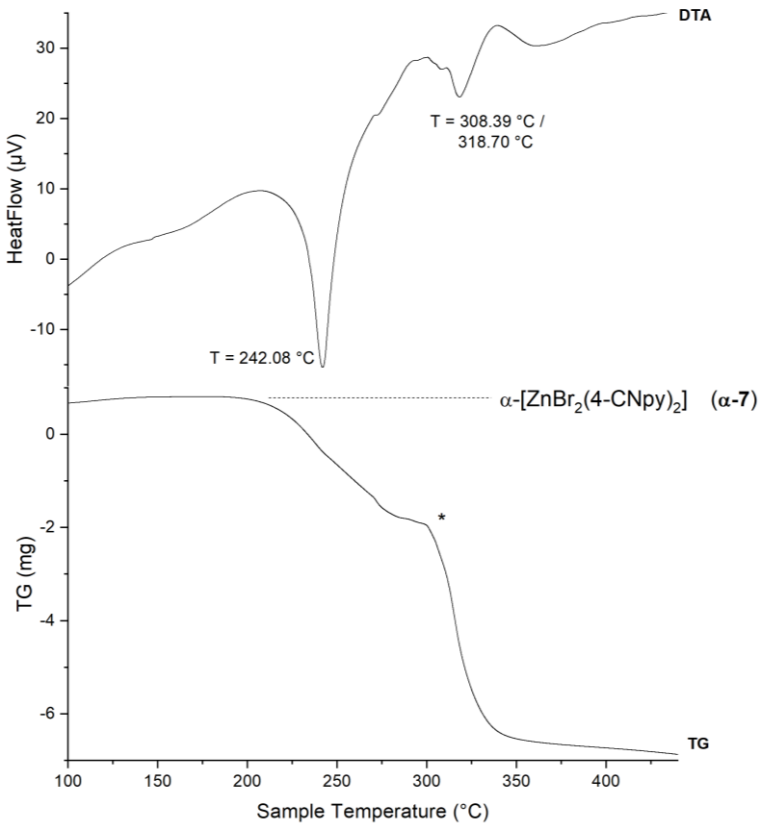

Figure S6. DTA/TG curves of α-[$ZnBr_2$(4-CNpy)$_2$] (**α-7**). The star * marks a phase of unknown composition. Heating rate: 5 K/min, Ar atmosphere, Al_2O_3 crucible.

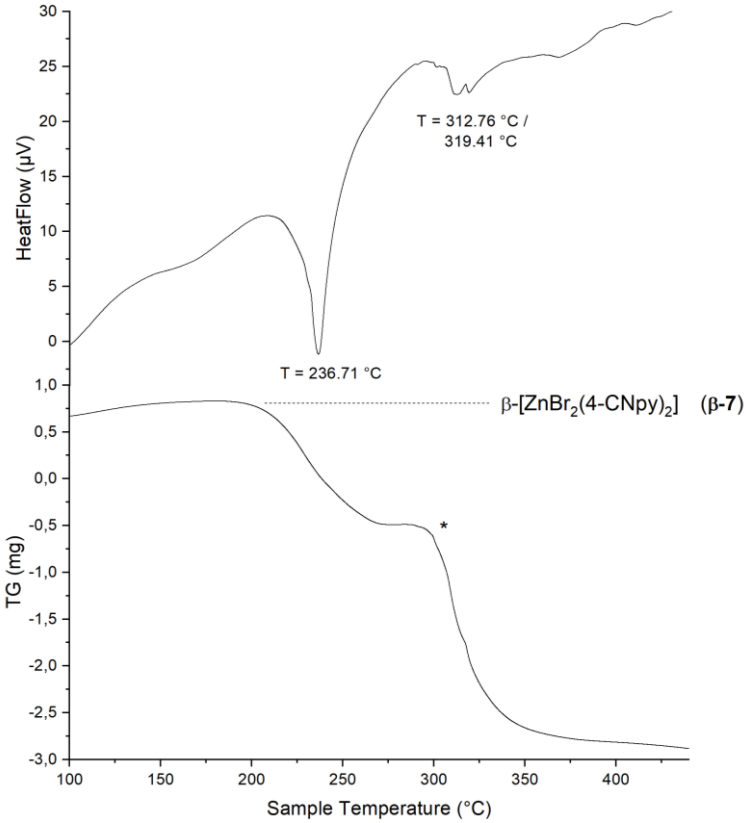

Figure S7. DTA/TG curves of β-[$ZnBr_2$(4-CNpy)$_2$] (**β-7**). The star * marks a phase of unknown composition. Heating rate: 5 K/min, Ar atmosphere, Al_2O_3 crucible.

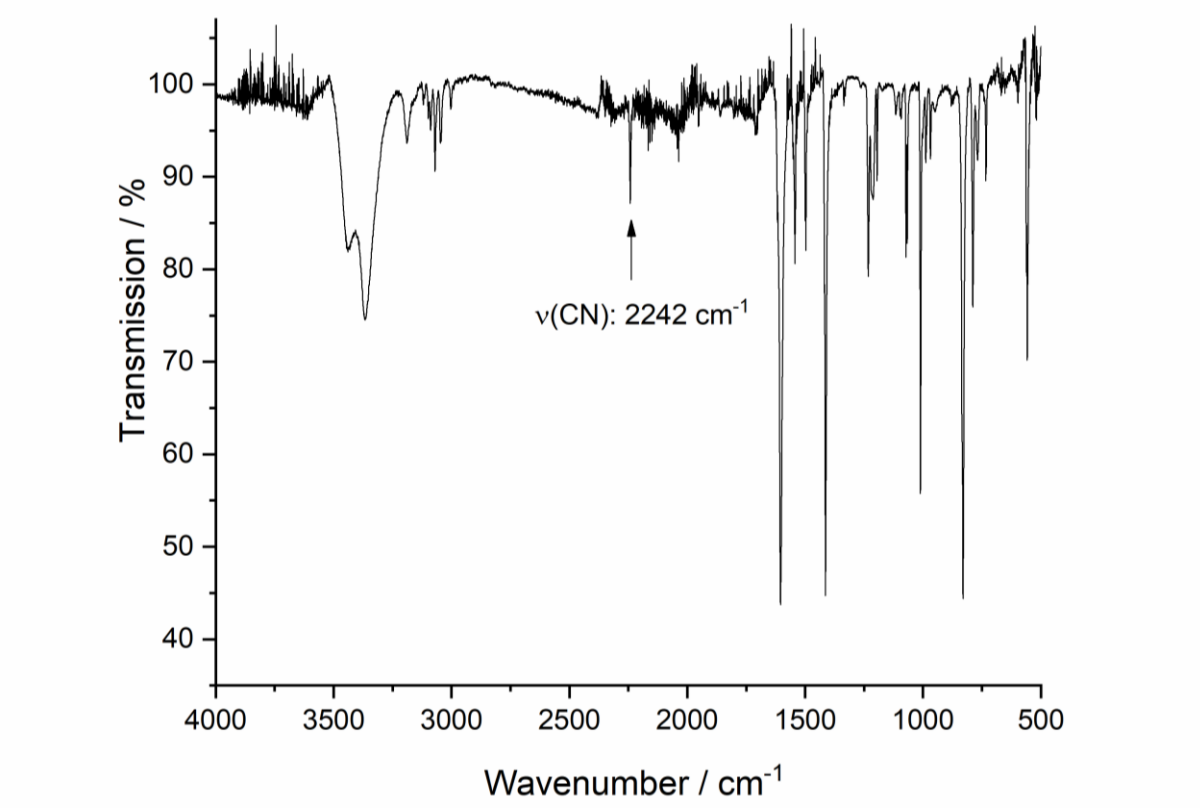

Figure S8. IR spectrum of α-[$MnBr_2$(4-CNpy)$_2$]$_n$ (**α-1a**).

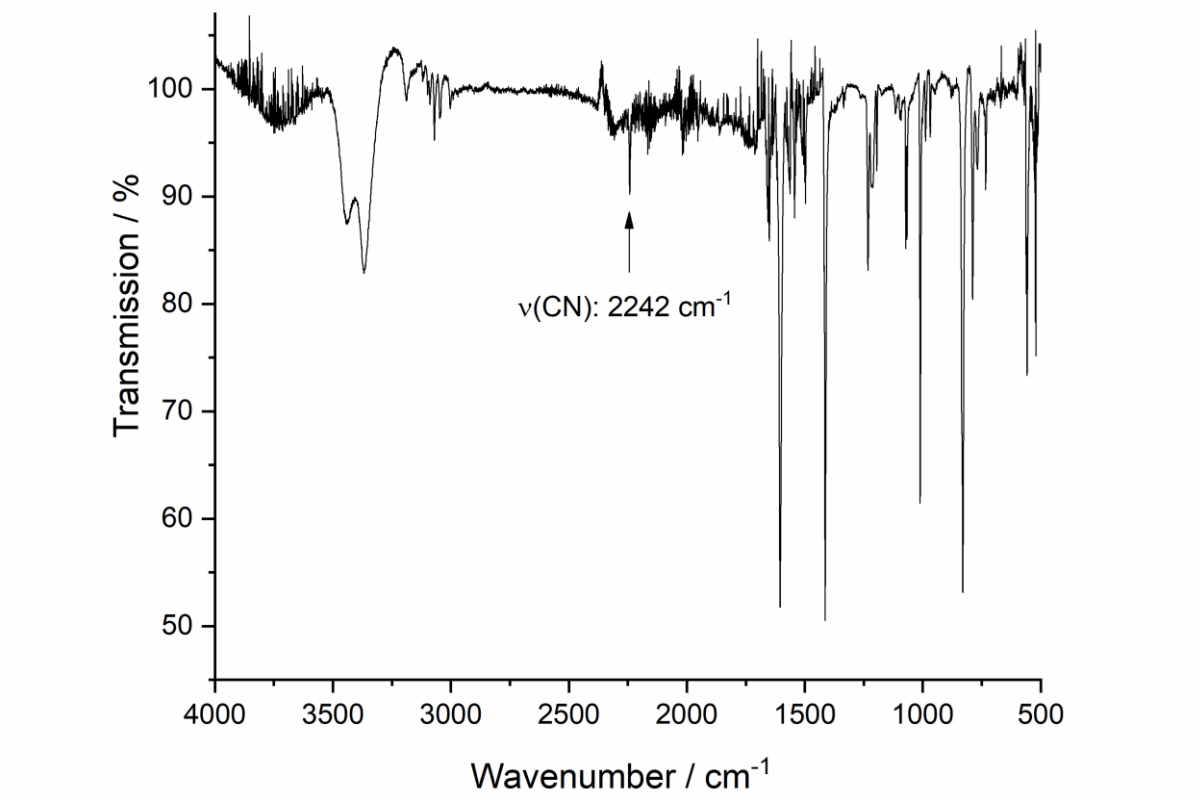

Figure S9. IR spectrum of β-[$MnBr_2$(4-CNpy)$_2$]$_n$ (**β-1a**).

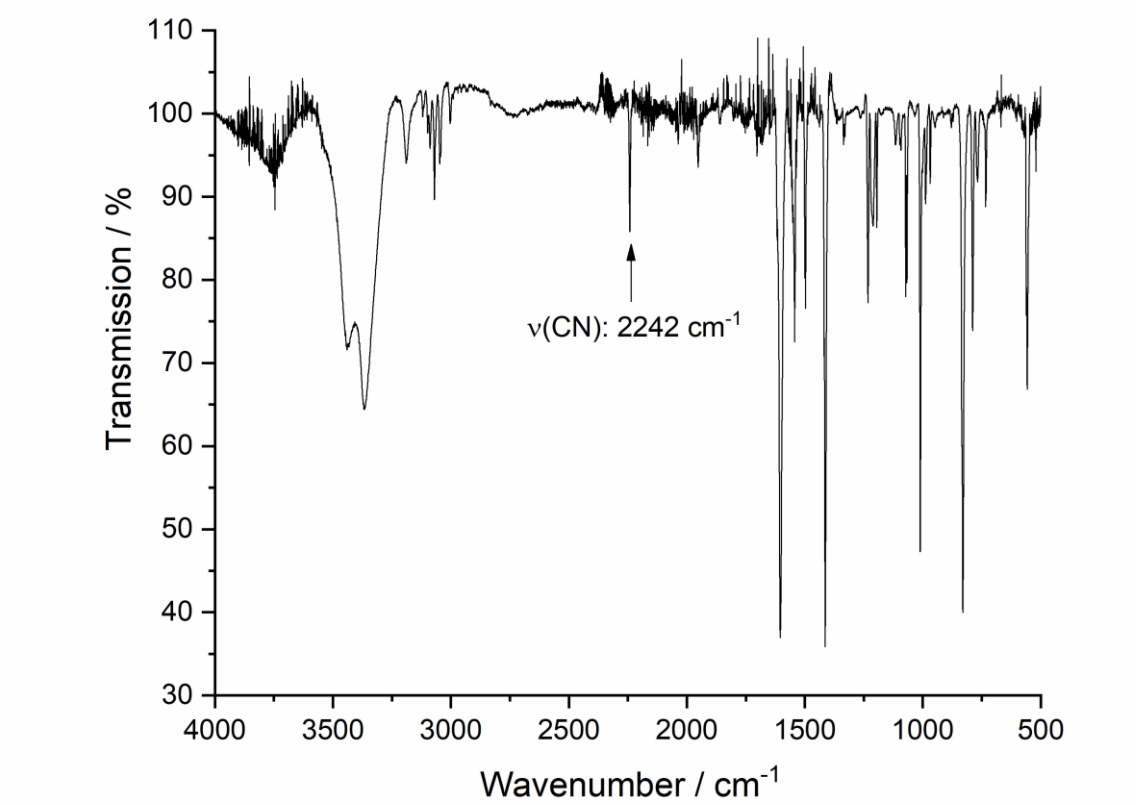

Figure S10. IR spectrum of $[MnBr_2(4\text{-}CNpy)_1]_n$ (**1b**).

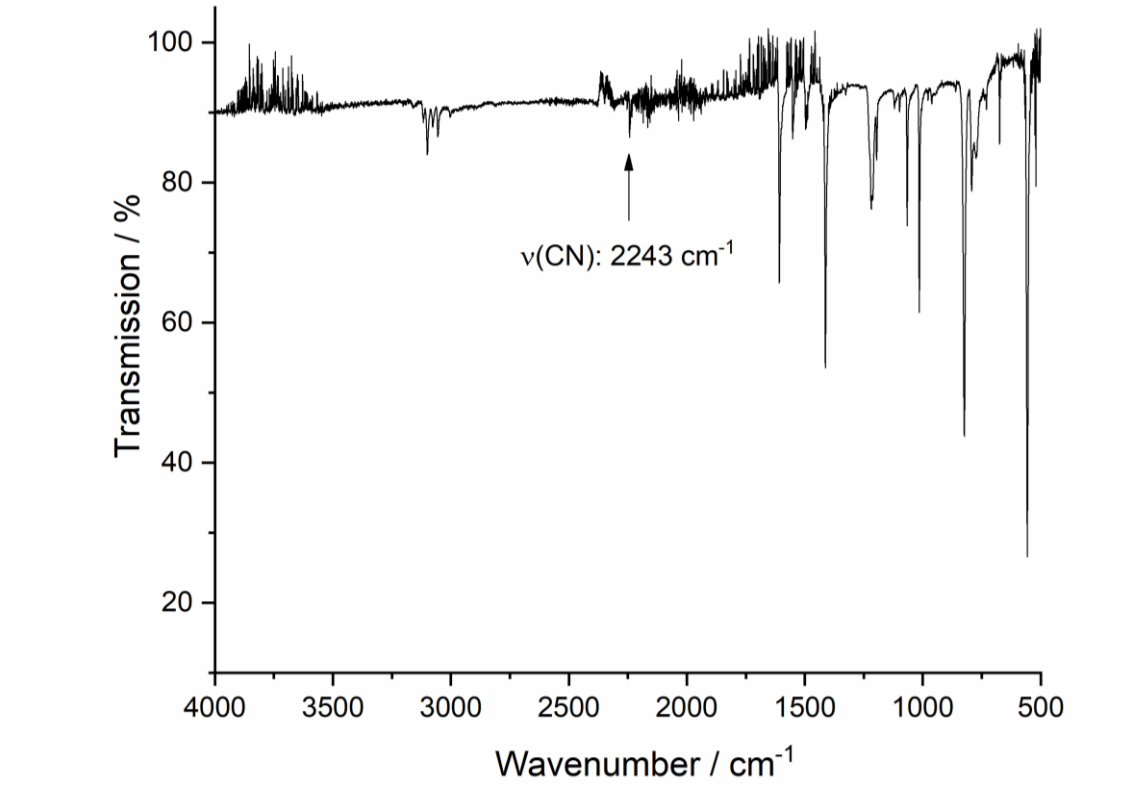

Figure S11. IR spectrum of $[FeCl_2(4\text{-}CNpy)_2]_n$ (**2a**).

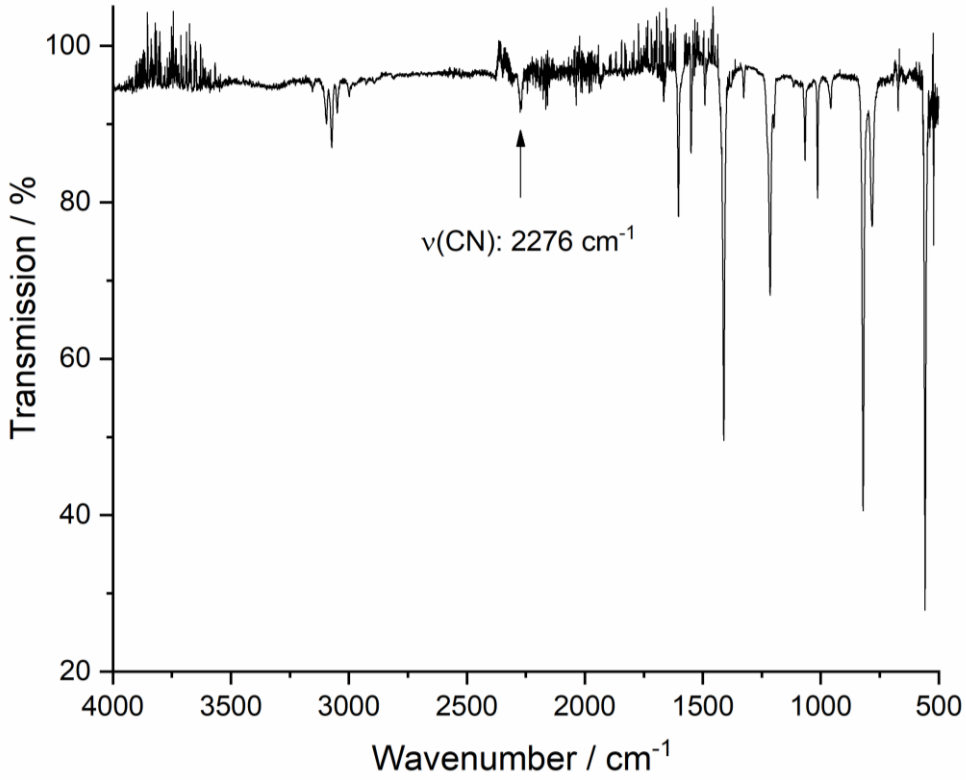

Figure S12. IR spectrum of $[FeCl_2(4\text{-}CNpy)_1]_n$ (**2b**).

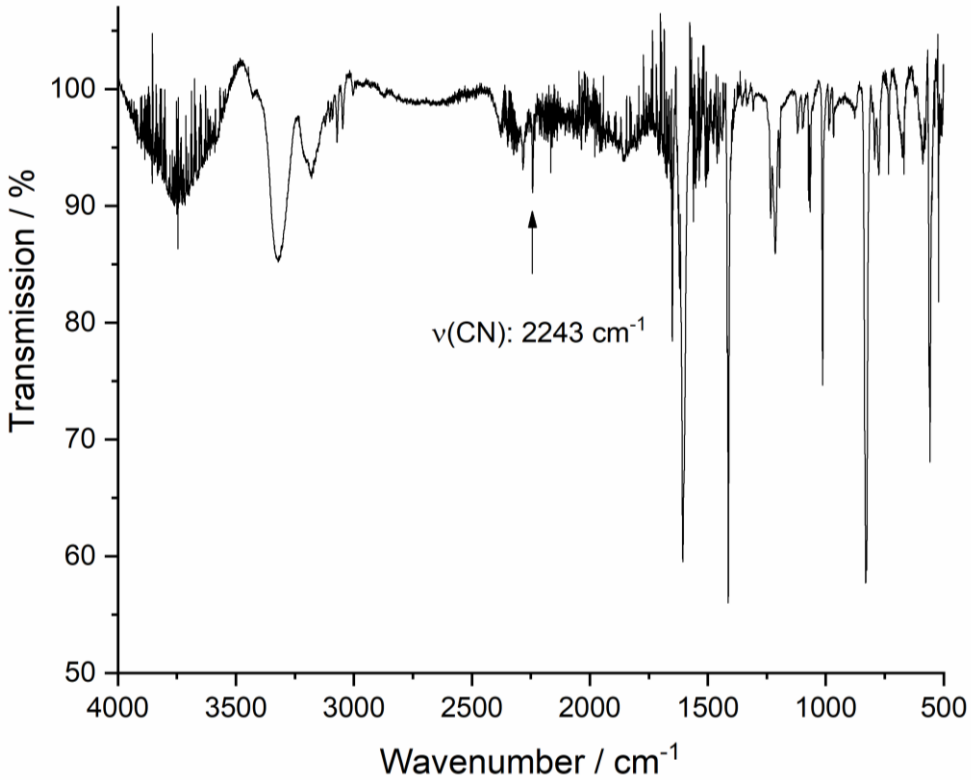

Figure S13. IR spectrum of $[FeBr_2(4\text{-}CNpy)_2]_n$ (**3a**).

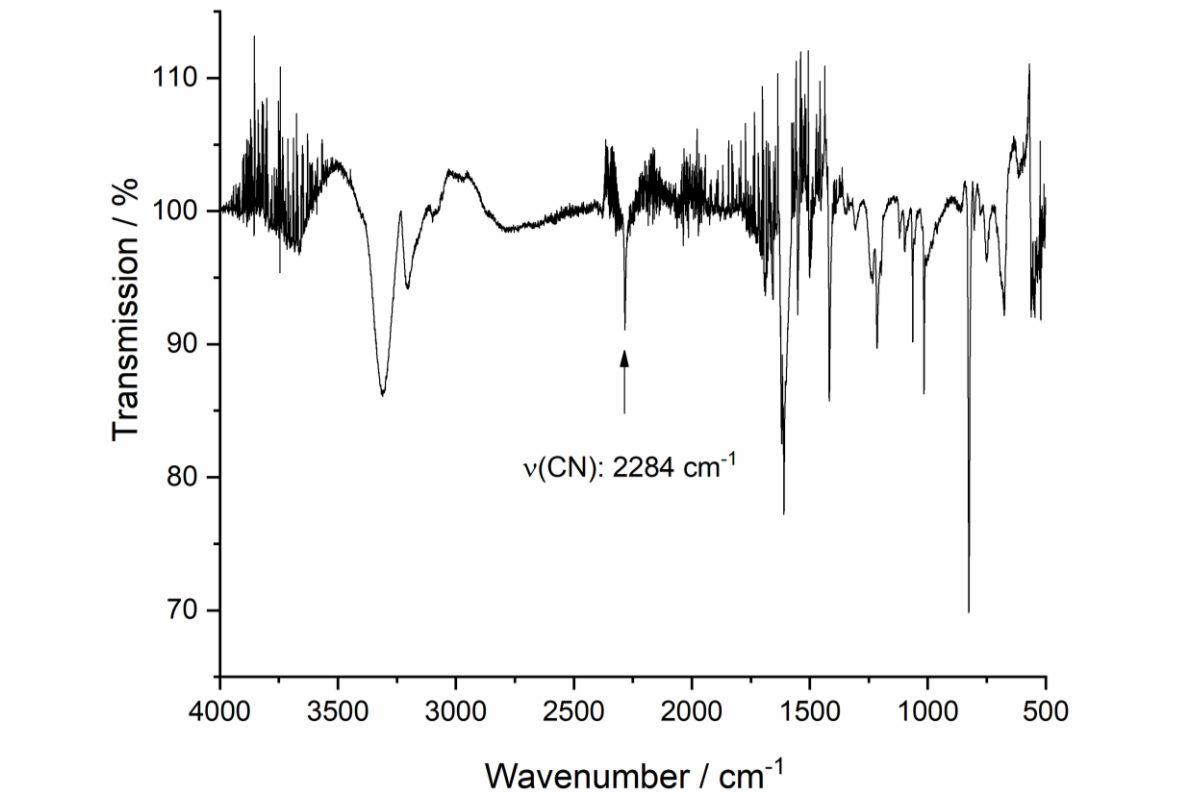

Figure S14. IR spectrum of $[FeBr_2(4\text{-CNpy})_1]_n$ (**3b**).

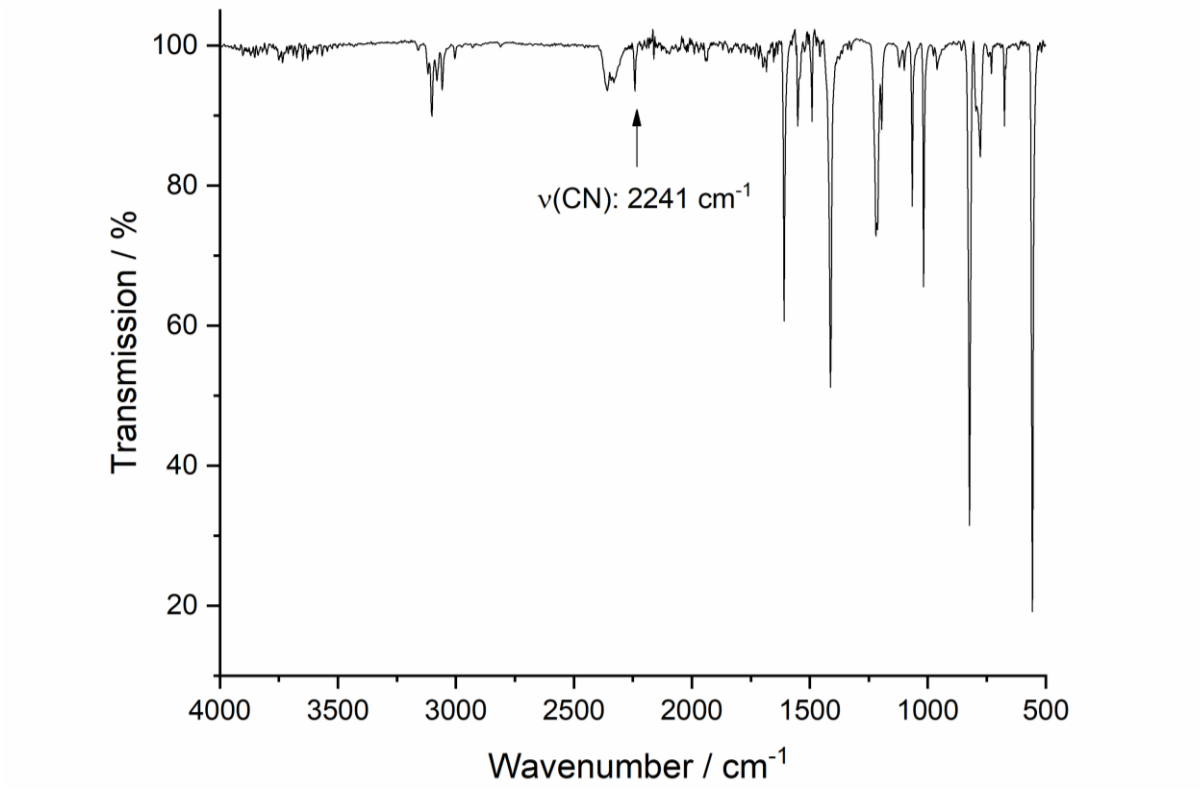

Figure S15. IR spectrum of $[CoCl_2(4\text{-CNpy})_2]_n$ (**4a**).

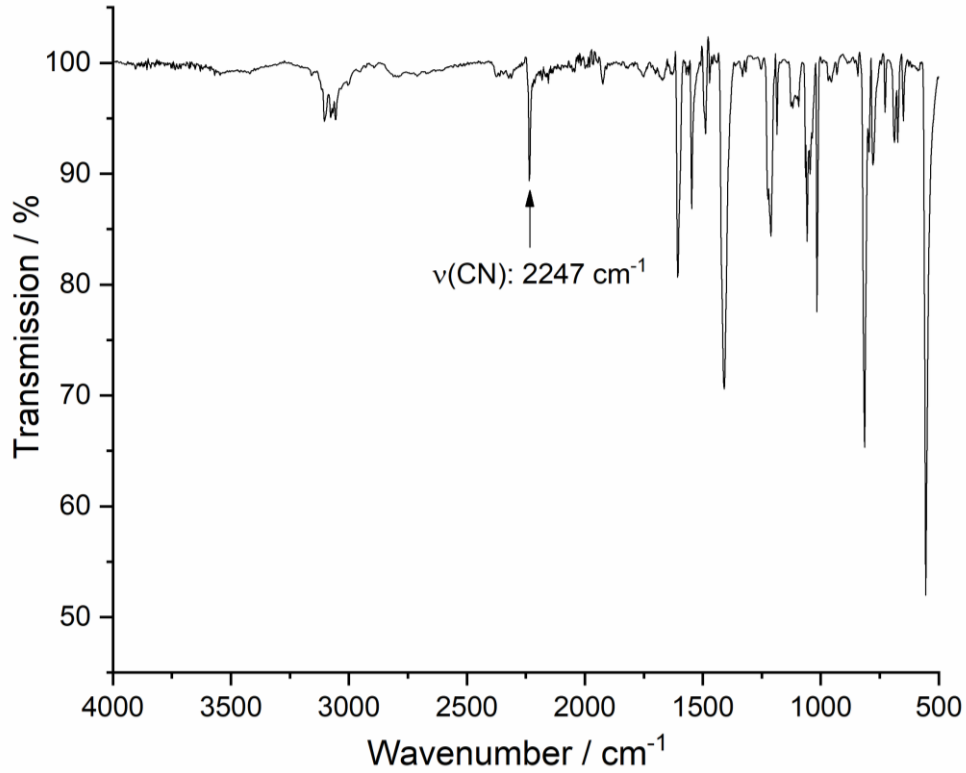

Figure S16. IR spectrum of $[CoBr_2(4\text{-}CNpy)_2]_n$ (**5a**).

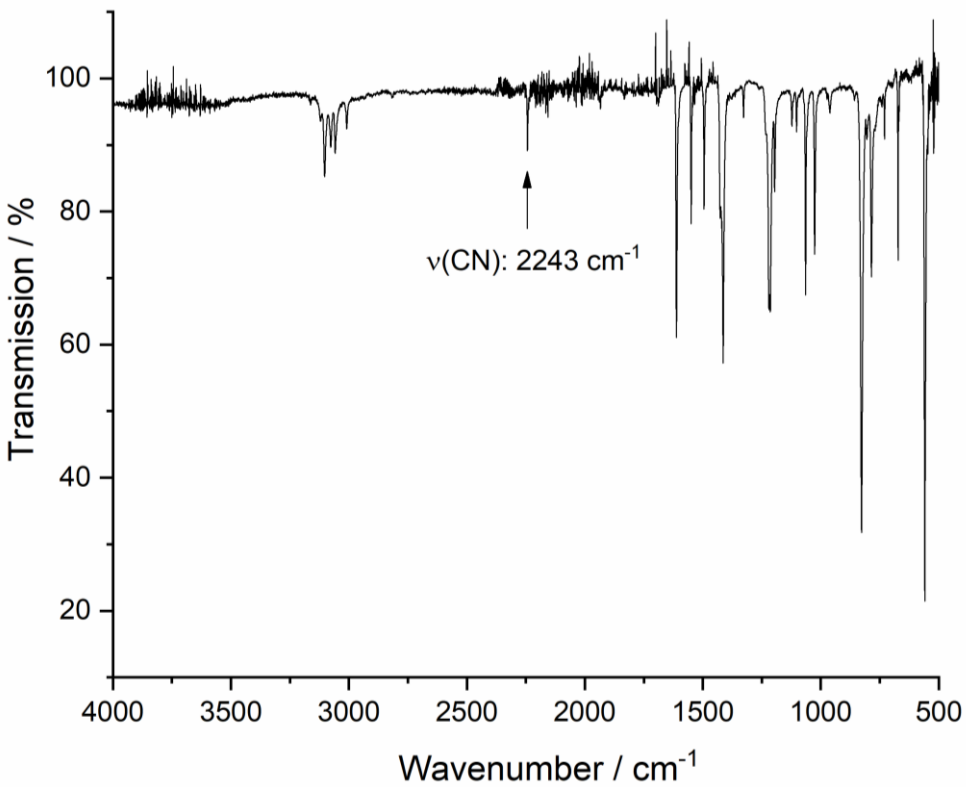

Figure S17. IR spectrum of $[CuBr_2(4\text{-}CNpy)_2]_n$ (**6**).

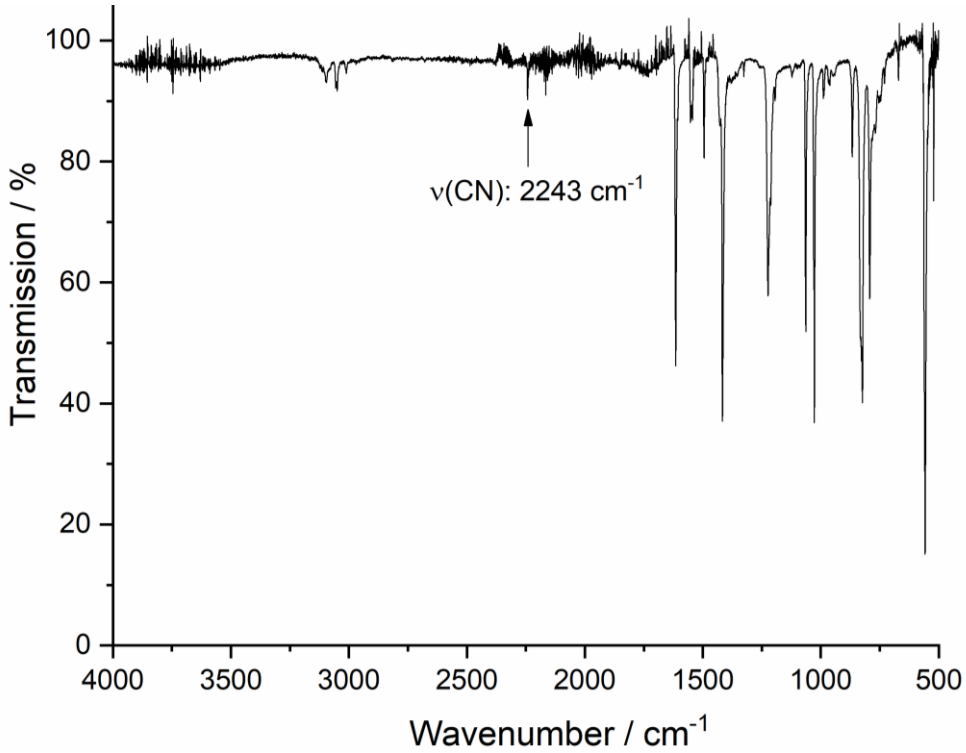

Figure S18. IR spectrum of α-[$ZnBr_2$(4-CNpy)$_2$] (**α-7**).

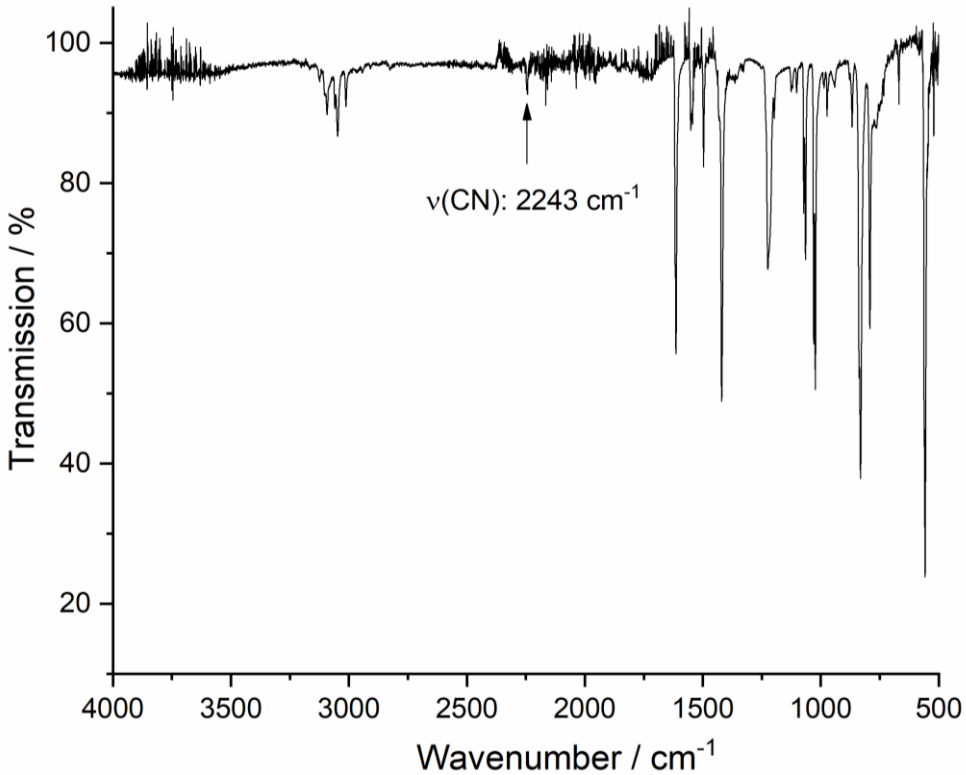

Figure S19. IR spectrum of β-[$ZnBr_2$(4-CNpy)$_2$] (**β-7**).

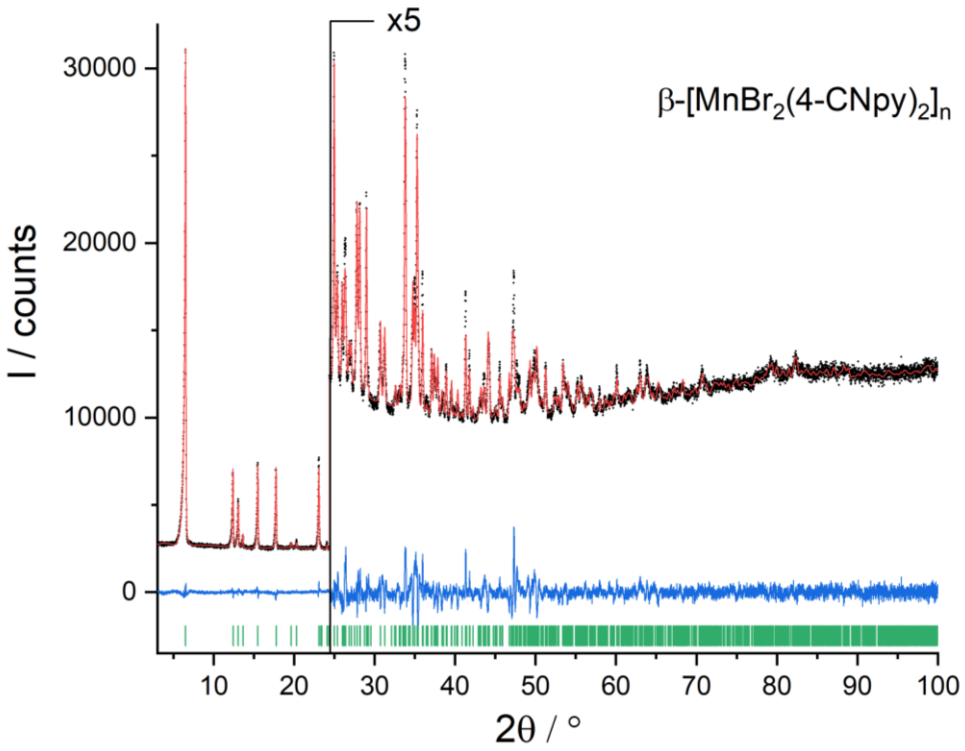

Figure S20. Rietveld plot of (**β-1a**). Observed powder diagram (black points), calculated powder diagram (red solid line), difference curve (blue solid line) and calculated reflection positions (green bars). Change of the scales with corresponding factor is indicated.

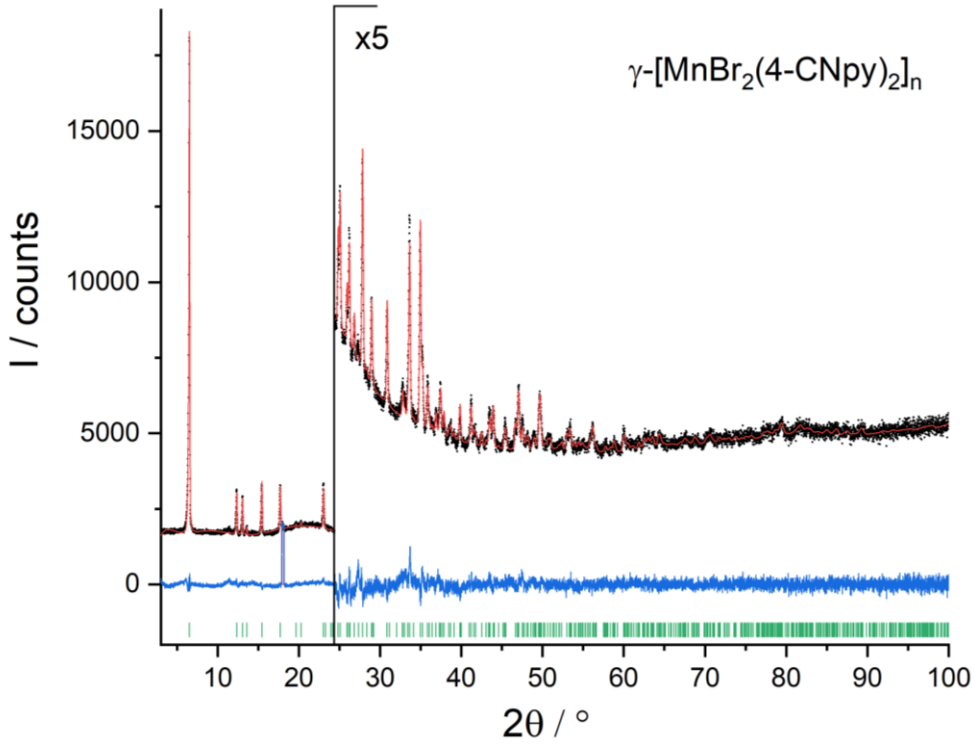

Figure S21. Rietveld plot of (**γ-1a**). Observed powder diagram (black points), calculated powder diagram (red solid line), difference curve (blue solid line) and calculated reflection positions (green bars). One appearing reflection of **1b** was excluded during the refinement. Change of the scales with corresponding factor is indicated.

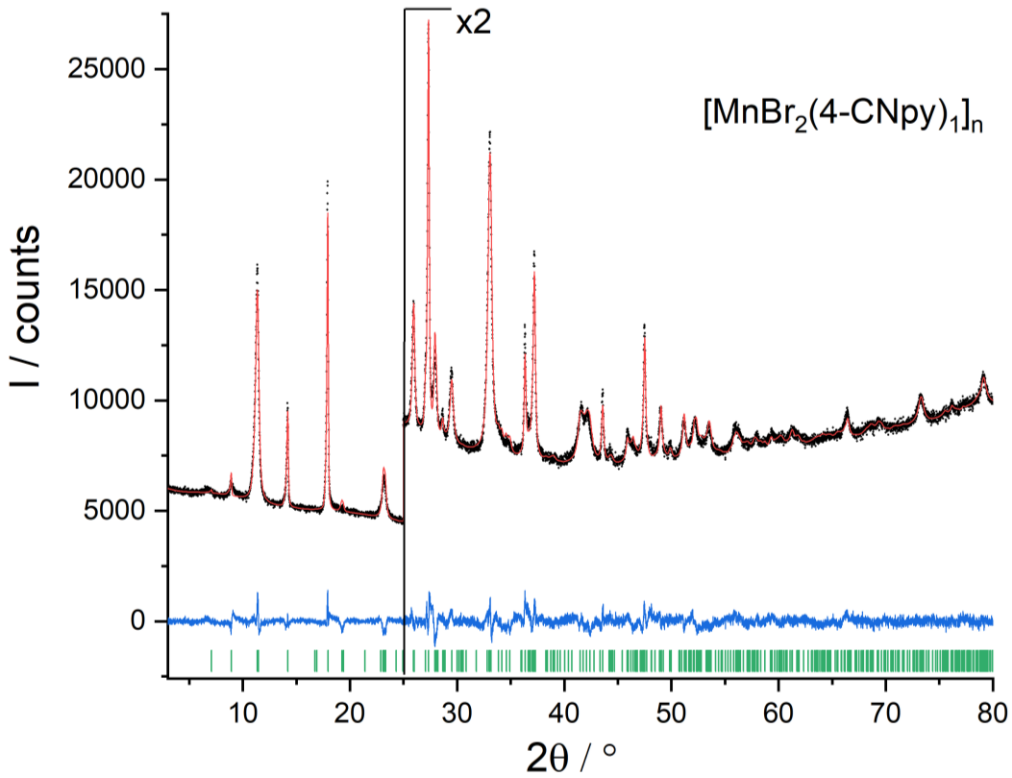

Figure S22. Rietveld plot of (**1b**). Observed powder diagram (black points), calculated powder diagram (red solid line), difference curve (blue solid line) and calculated reflection positions (green bars). Change of the scales with corresponding factor is indicated.

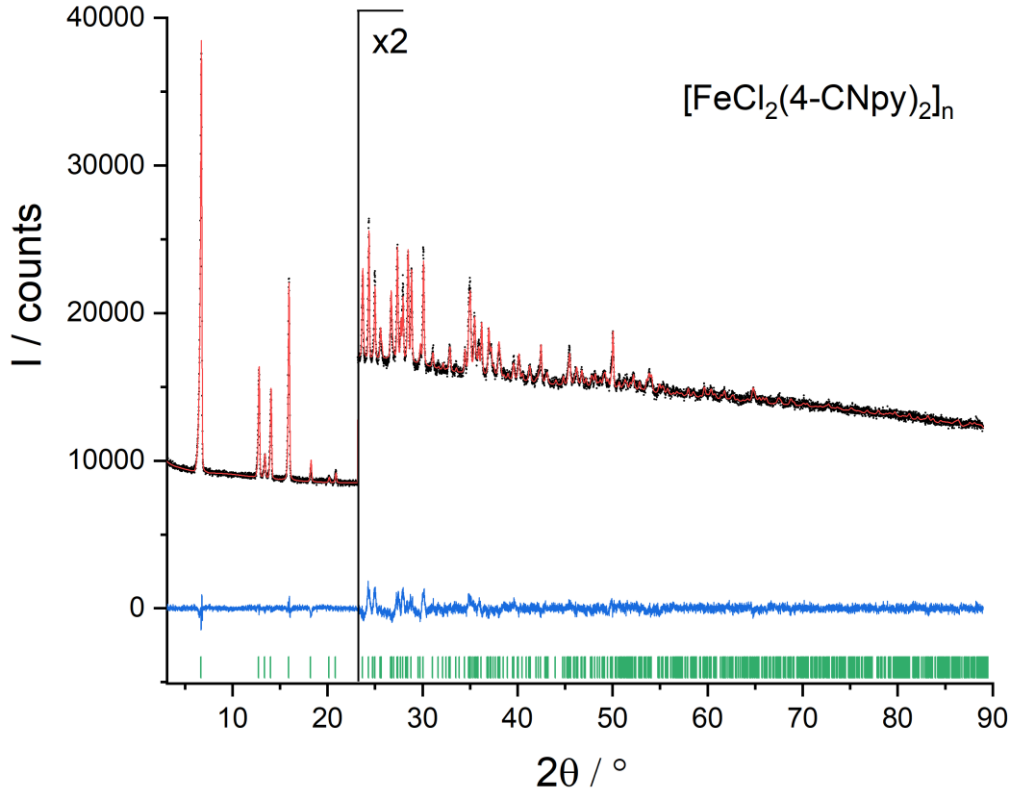

Figure S23. Rietveld plot of (**2a**). Observed powder diagram (black points), calculated powder diagram (red solid line), difference curve (blue solid line) and calculated reflection positions (green bars). Change of the scales with corresponding factor is indicated.

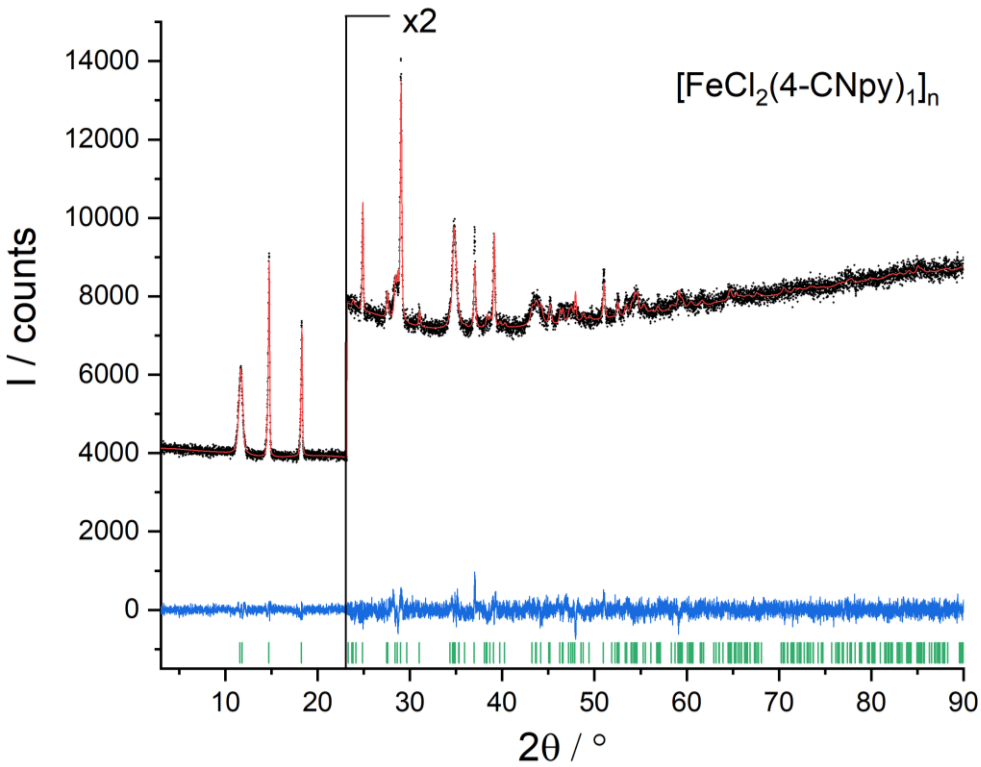

Figure S24. Rietveld plot of (**2b**). Observed powder diagram (black points), calculated powder diagram (red solid line), difference curve (blue solid line) and calculated reflection positions (green bars). Change of the scales with corresponding factor is indicated.

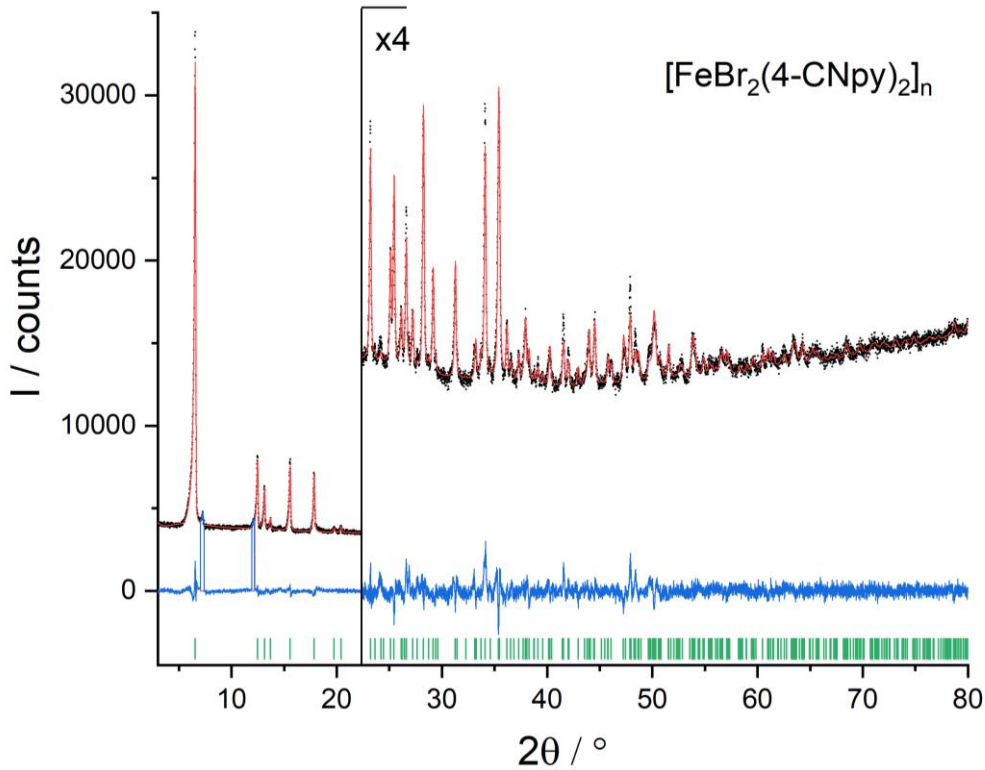

Figure S25. Rietveld plot of (**3a**). Observed powder diagram (black points), calculated powder diagram (red solid line), difference curve (blue solid line) and calculated reflection positions (green bars). Reflections of a foreign phase are excluded. Change of the scales with corresponding factor is indicated

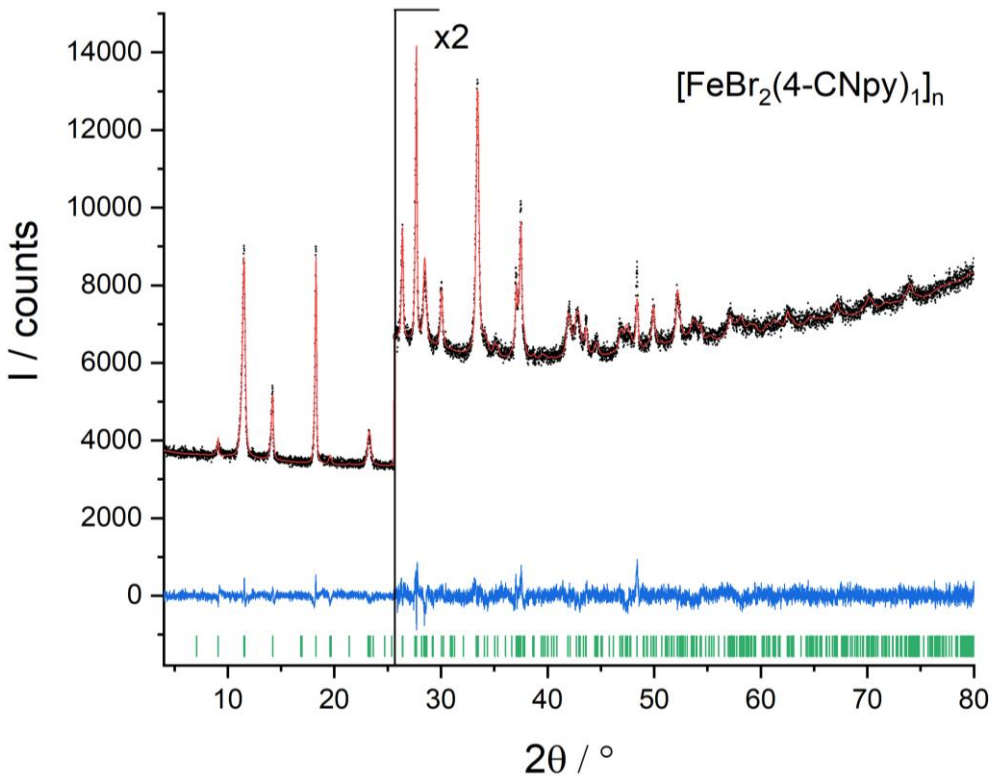

Figure S26. Rietveld plot of (**3b**). Observed powder diagram (black points), calculated powder diagram (red solid line), difference curve (blue solid line) and calculated reflection positions (green bars). Change of the scales with corresponding factor is indicated.

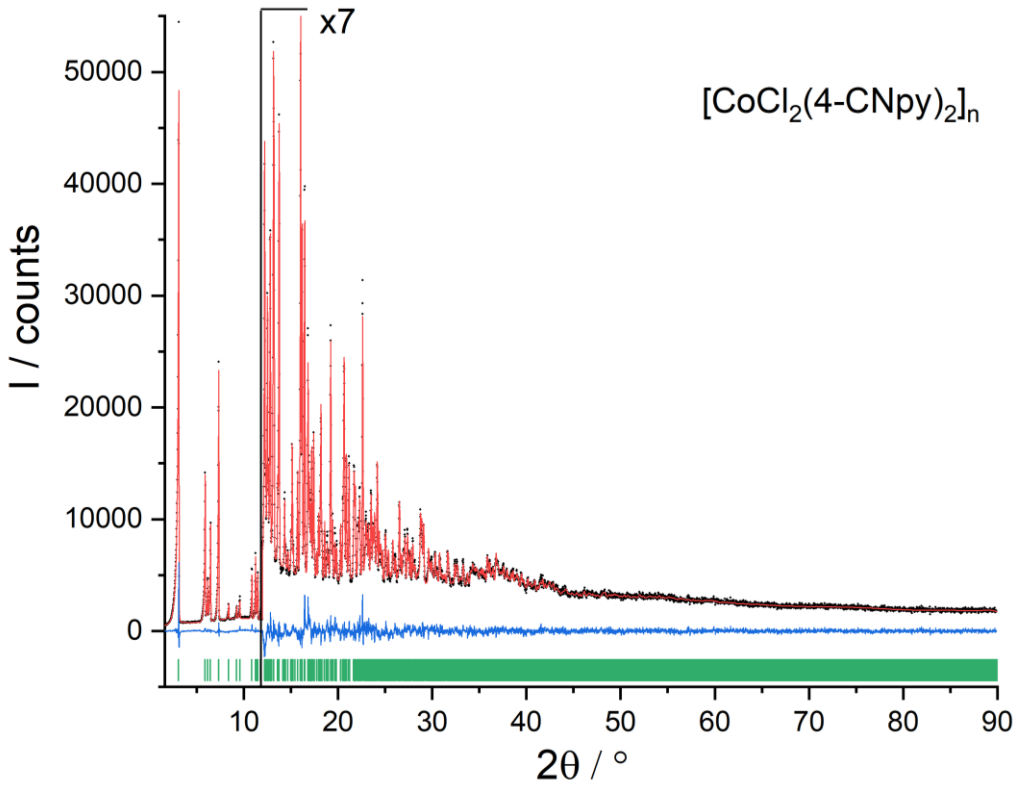

Figure S27a. Full Rietveld plot of (**4a**). Observed powder diagram (black points), calculated powder diagram (red solid line), difference curve (blue solid line) and calculated reflection positions (green bars). Change of the scales with corresponding factor is indicated.

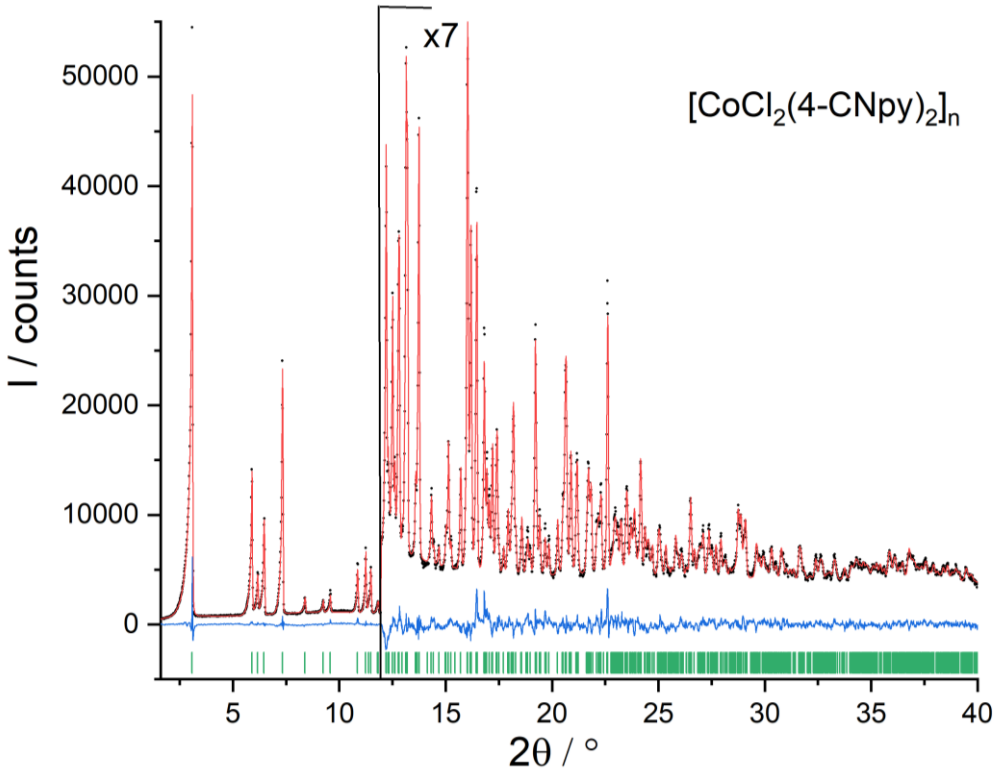

Figure S27b. Rietveld plot of (**4a**) shown until 40° in 2θ. Observed powder diagram (black points), calculated powder diagram (red solid line), difference curve (blue solid line) and calculated reflection positions (green bars). Change of the scales with corresponding factor is indicated.

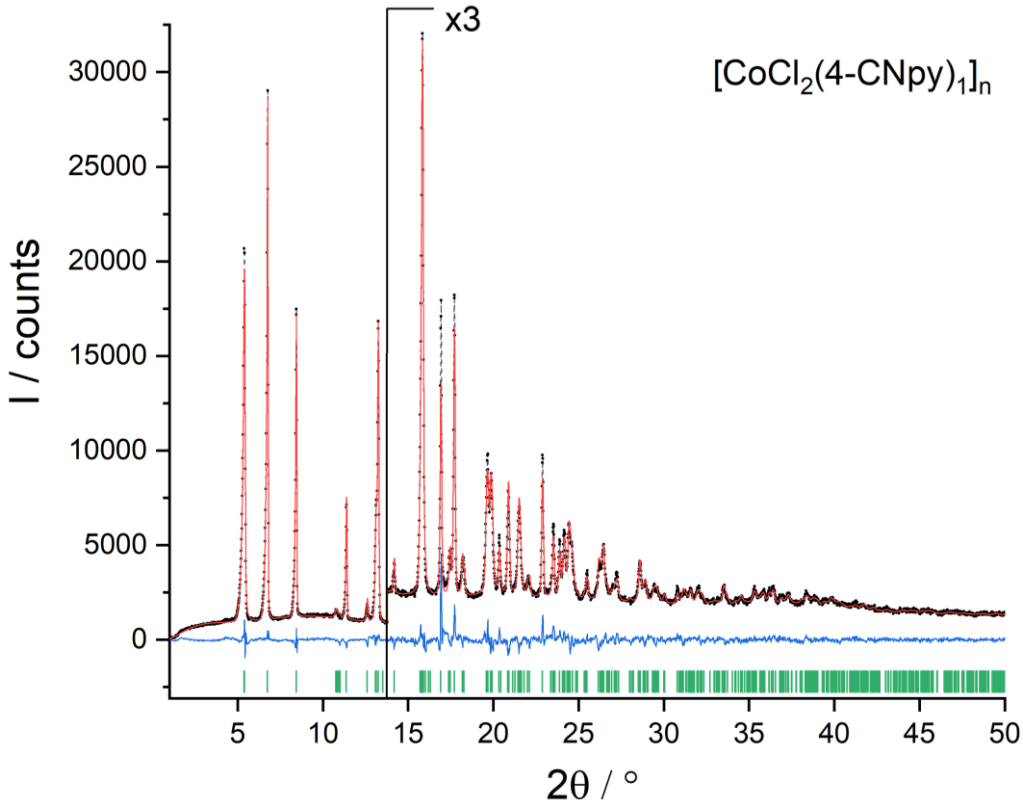

Figure S28. Rietveld plot of (**4b**). Observed powder diagram (black points), calculated powder diagram (red solid line), difference curve (blue solid line) and calculated reflection positions (green bars). Change of the scales with corresponding factor is indicated.

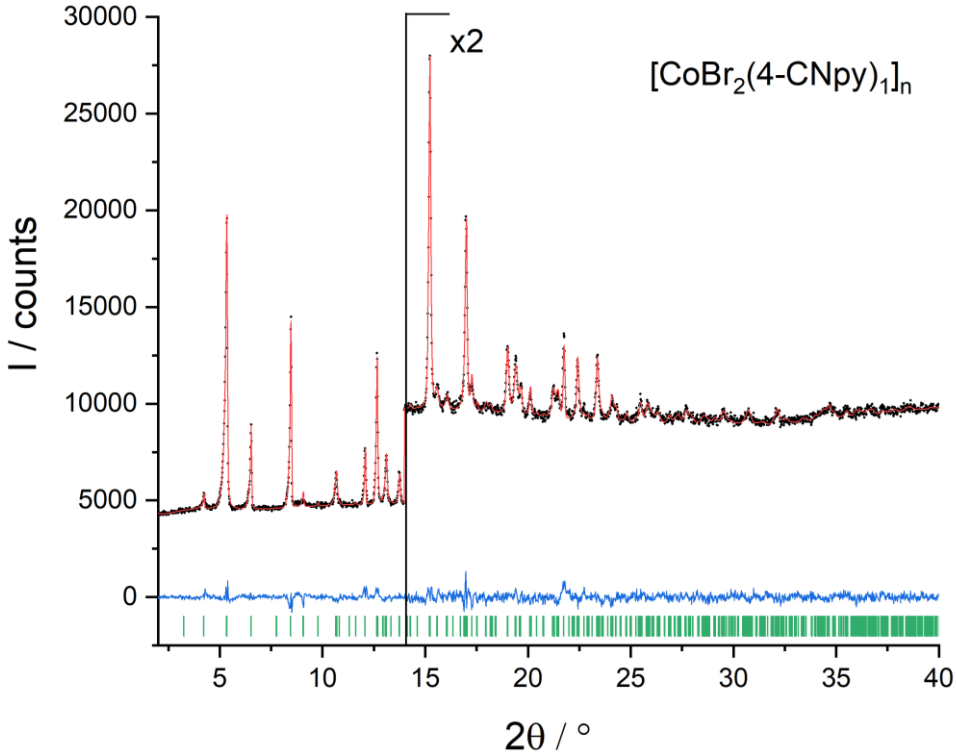

Figure S29. Rietveld plot of (**5b**). Observed powder diagram (black points), calculated powder diagram (red solid line), difference curve (blue solid line) and calculated reflection positions (green bars). Change of the scales with corresponding factor is indicated.

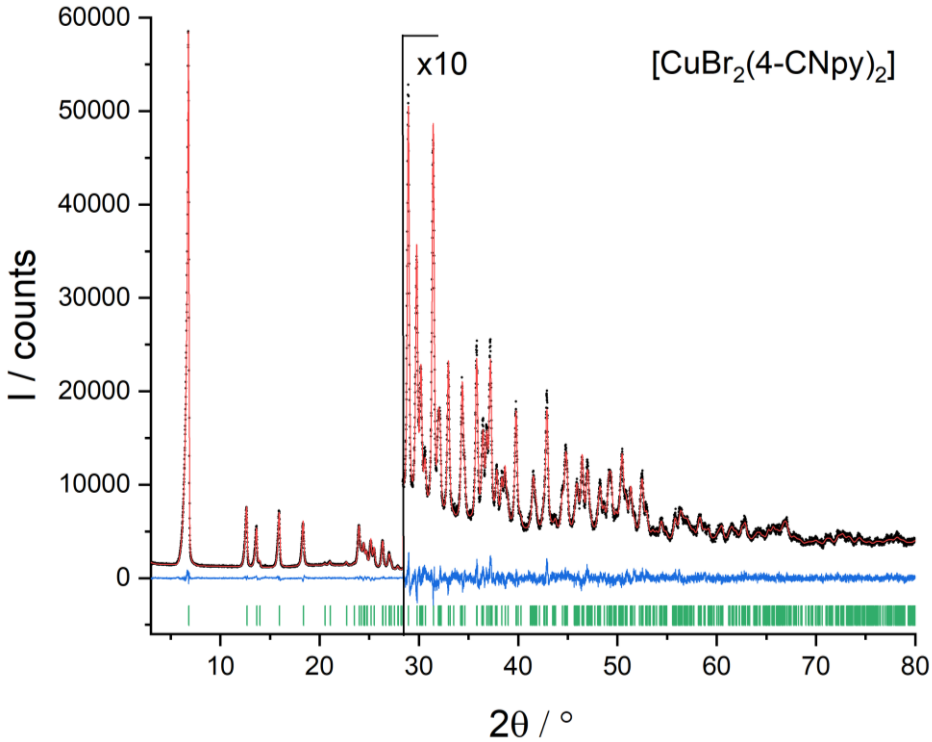

Figure S30. Rietveld plot of (**6**). Observed powder diagram (black points), calculated powder diagram (red solid line), difference curve (blue solid line) and calculated reflection positions (green bars). Change of the scales with corresponding factor is indicated.

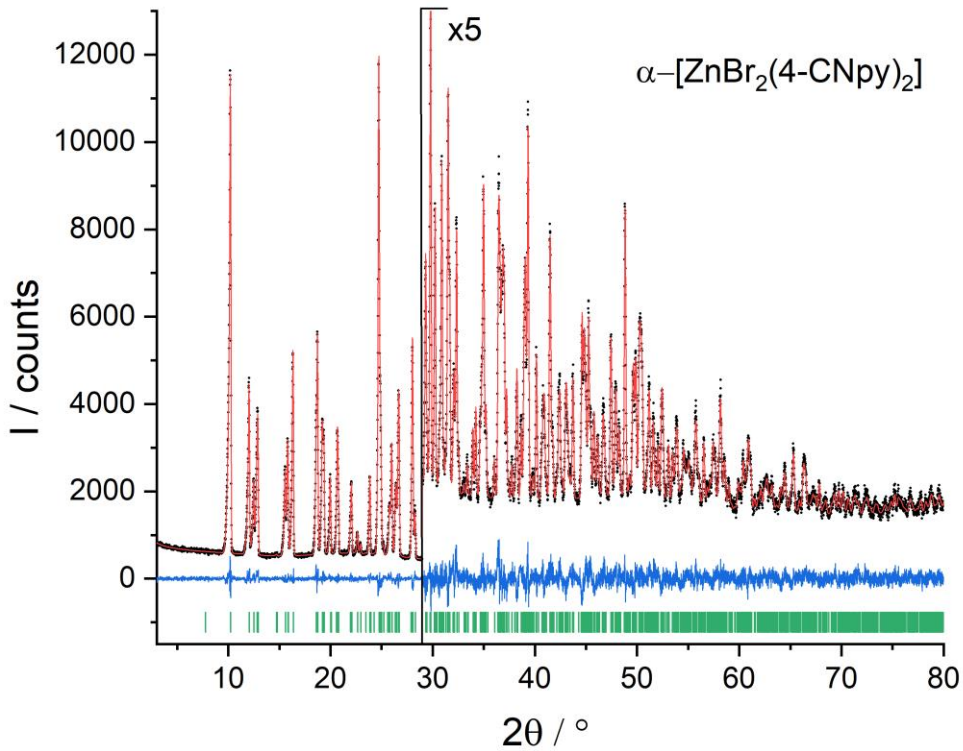

Figure S31. Rietveld plot of (**α-7**). Observed powder diagram (black points), calculated powder diagram (red solid line), difference curve (blue solid line) and calculated reflection positions (green bars). Change of the scales with corresponding factor is indicated.

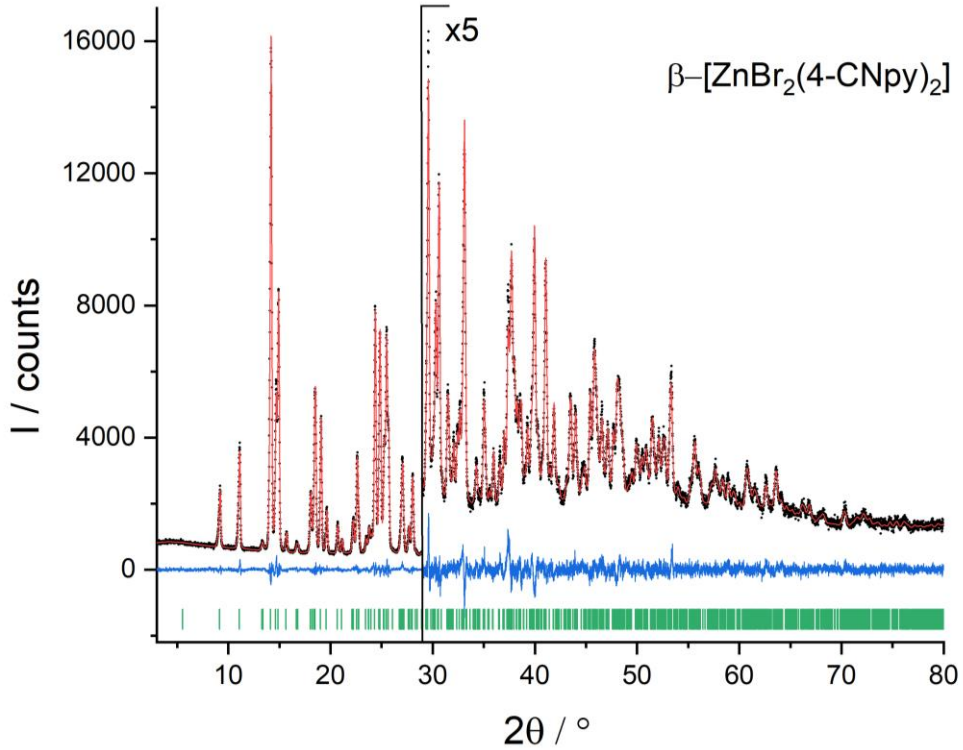

Figure S32. Rietveld plot of (**β-7**). Observed powder diagram (black points), calculated powder diagram (red solid line), difference curve (blue solid line) and calculated reflection positions (green bars). Change of the scales with corresponding factor is indicated.

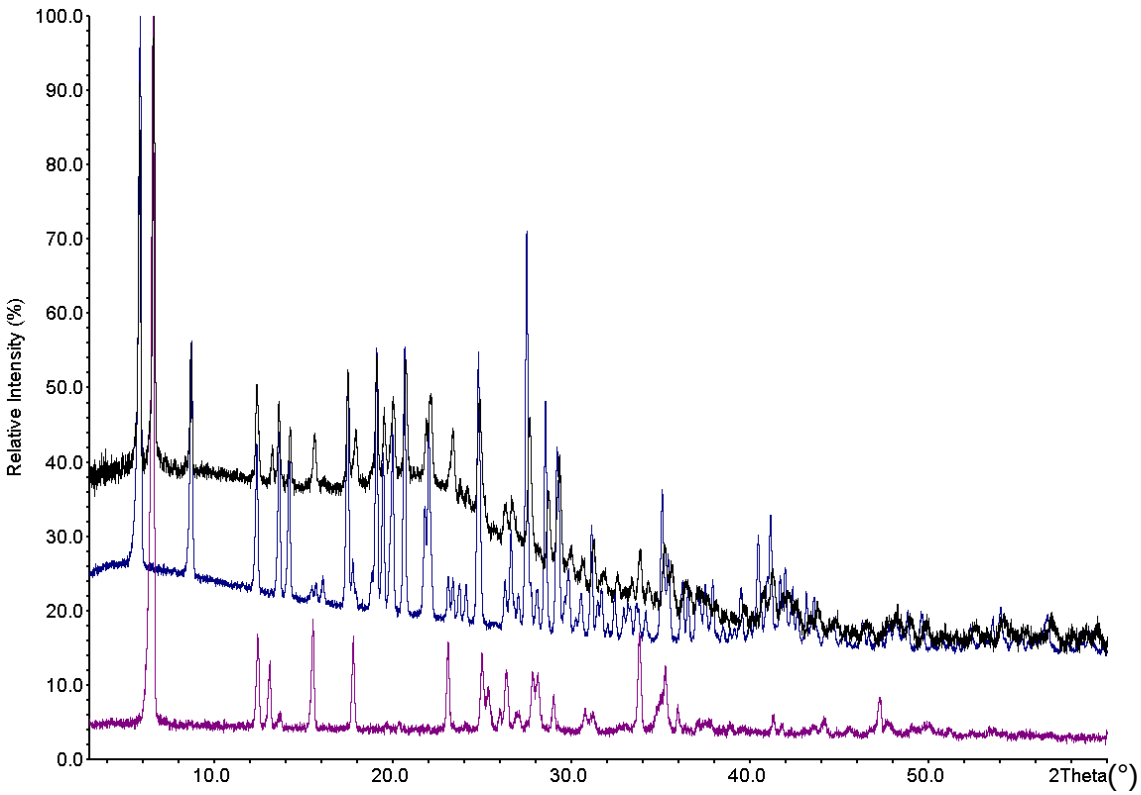

Figure S33. Experimental X-ray powder patterns of $[MnBr_2(4\text{-}CNpy)_2]_n$ (**1a**), collected with Cu-$K_{\alpha 1}$ radiation. Violet: initial room temperature measurement of **1a**: pure **β-1a**. Black: measurement of **1a** at -100°C: mixture of **α-1a** + **β-1a**. Blue: new room temperature measurement after several weeks of **1a:** pure **α-1a**.

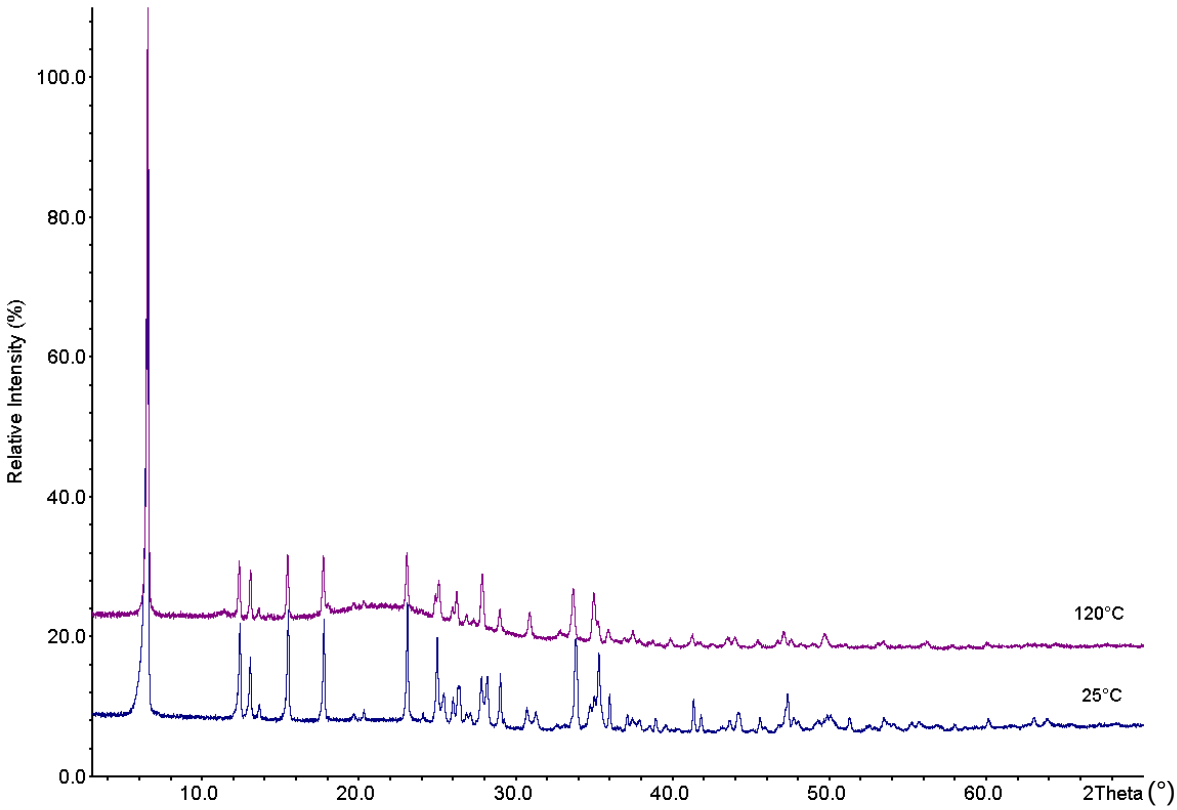

Figure S34. Experimental X-ray powder pattern of **β-1a** (blue) and **γ-1a** (violet), collected with Cu-$K_{\alpha 1}$ radiation.

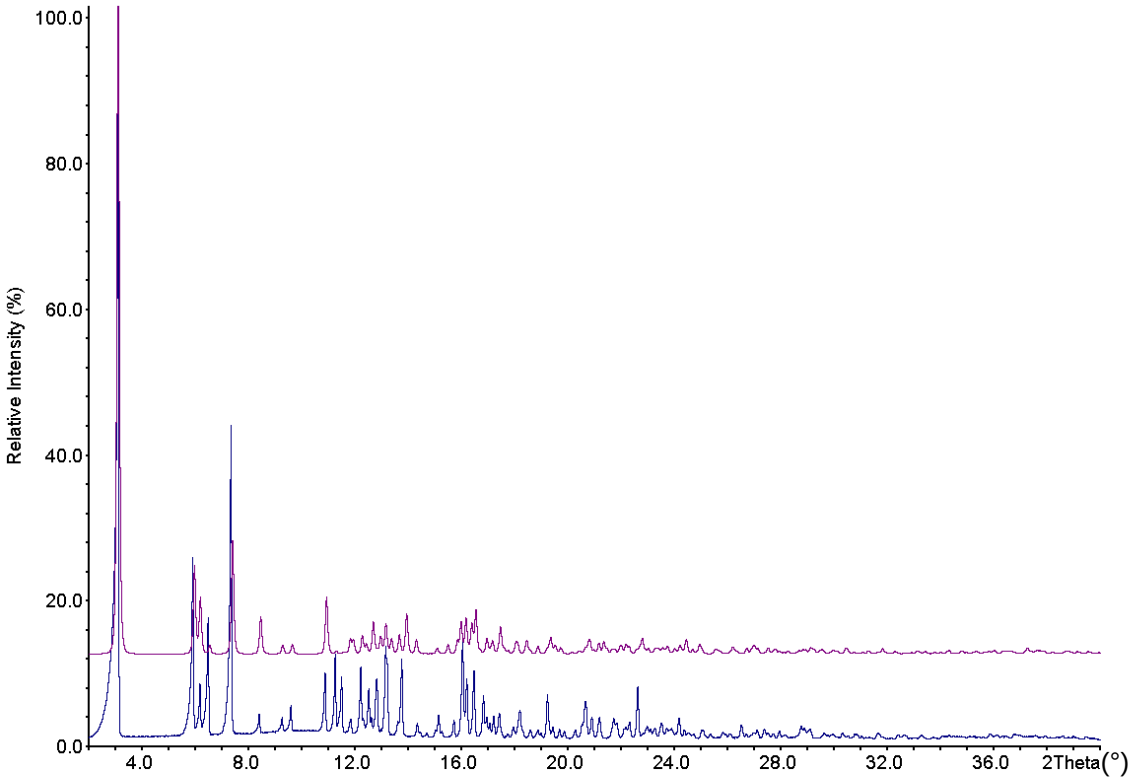

Figure S35. Experimental (blue) and calculated (UTIHIP, violet) X-ray powder pattern of $[CoCl_2(4\text{-}CNpy)_2]_n$ (**4a**) with Mo-$K_{\alpha1}$ radiation.

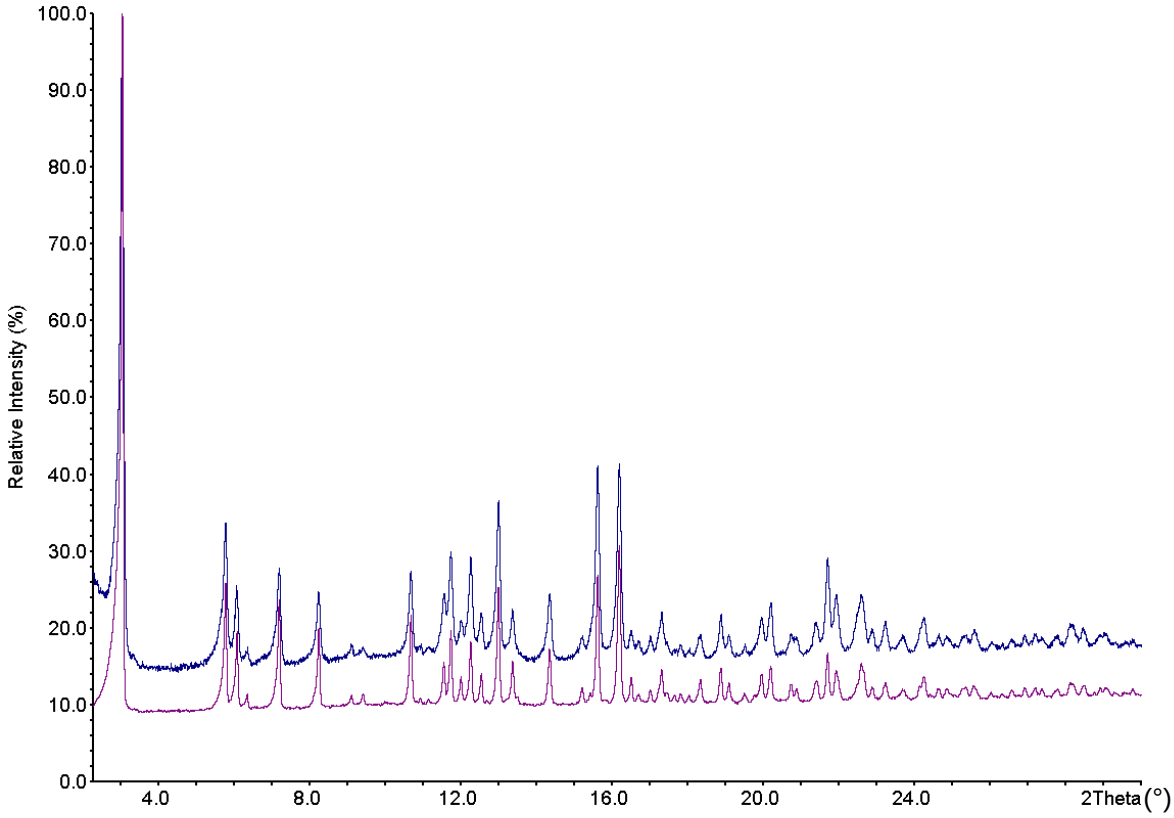

Figure S36. Experimental X-ray powder patterns of $[CoBr_2(4\text{-}CNpy)_2]_n$ (**5a**), collected with Mo-$K_{\alpha1}$ radiation. Blue: original data for structure determination of **5a** (LATJOI). Violet: data of a new sample of **5a**, obtained in 2019.

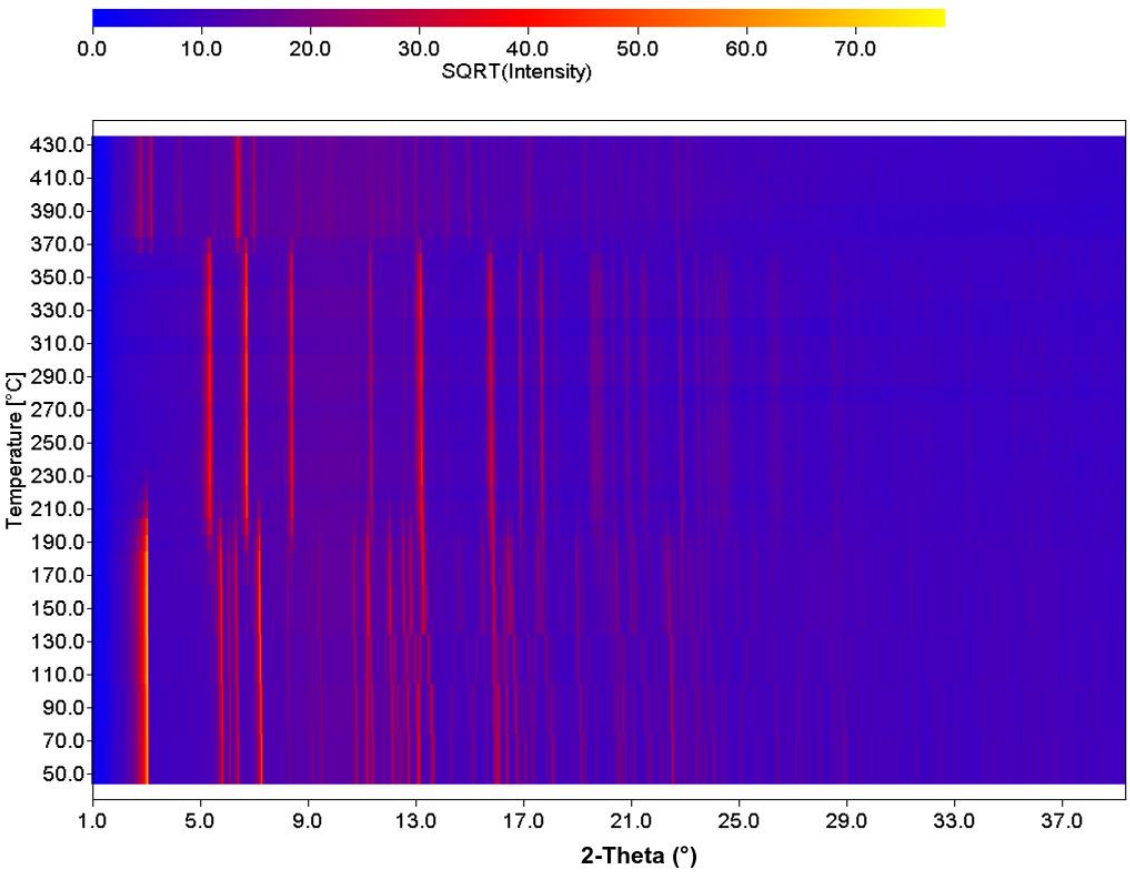

Figure S37. 3D-plot of the high-temperature X-ray measurement of $[CoCl_2(4\text{-}CNpy)_2]_n$ (**4a**), collected with Mo-$K_{\alpha1}$ radiation. Square root of the intensity chosen for better visibility.

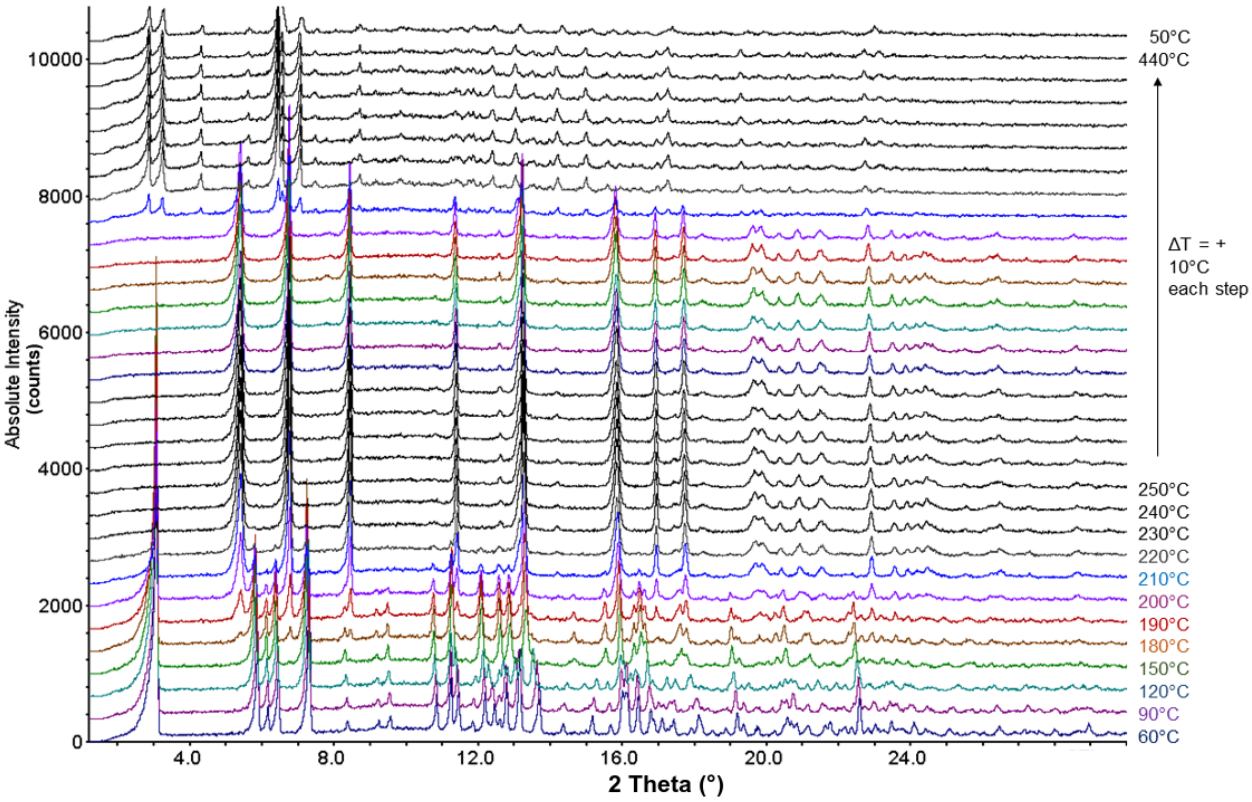

Figure S38. Temperature dependent X-ray powder pattern of **4a** transforming to **4b** and **4c,** collected with Mo-$K_{\alpha1}$ radiation.

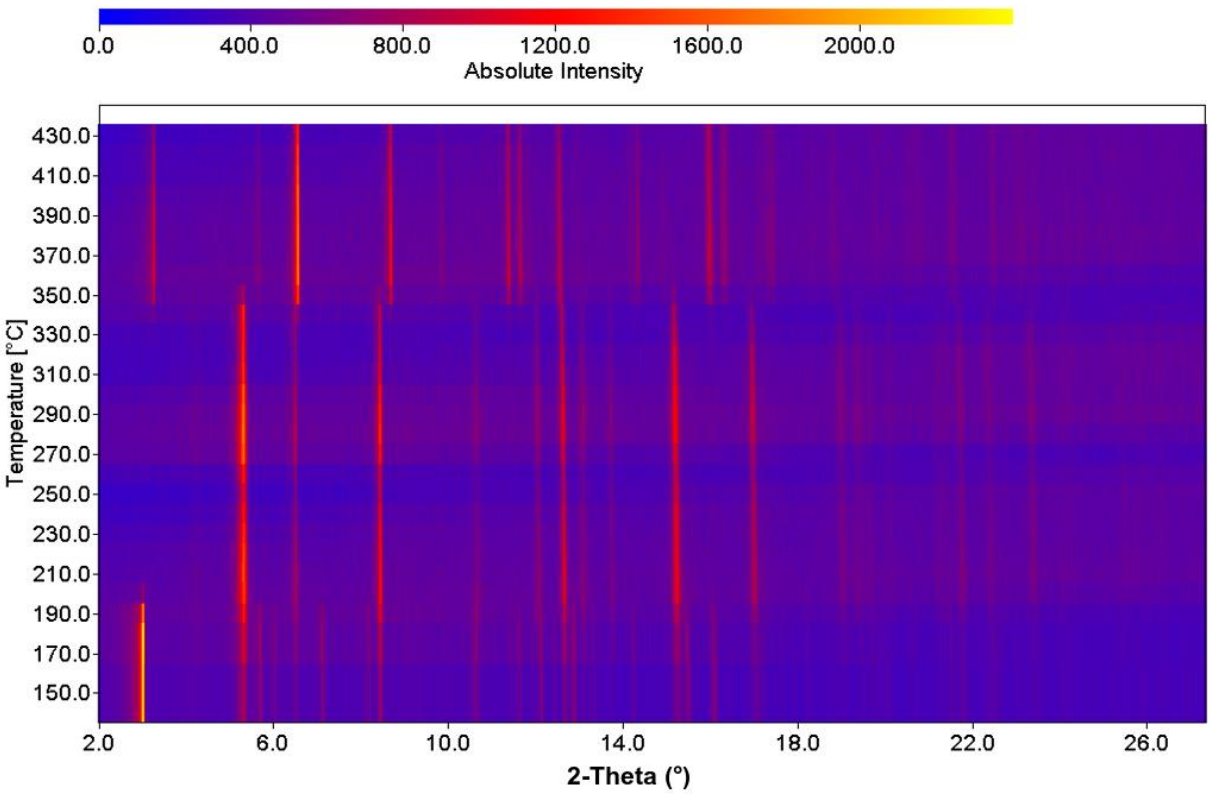

Figure S39. 3D-plot of the high-temperature X-ray measurement of $[CoBr_2(4\text{-}CNpy)_2]_n$ (**5a**), collected with Mo-$K_{\alpha1}$ radiation.

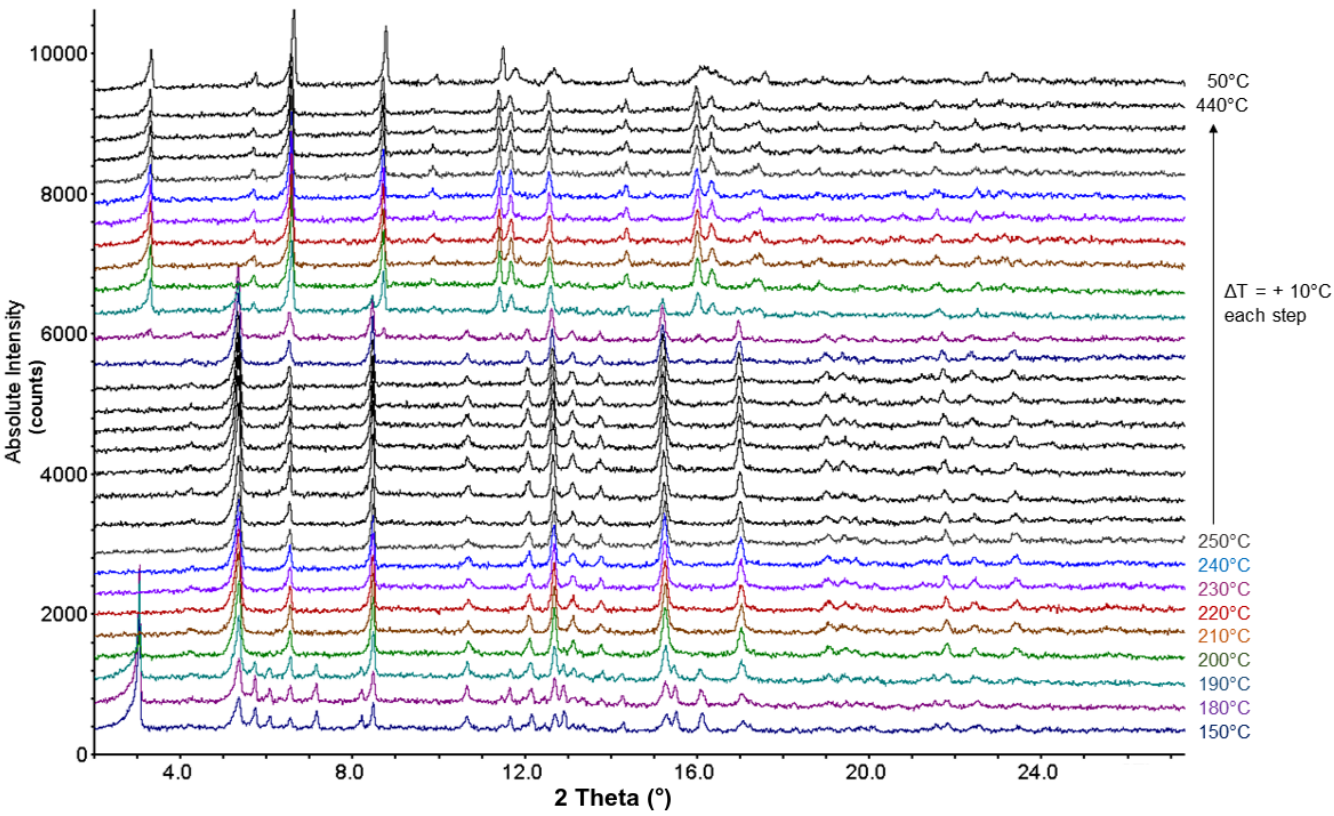

Figure S40. Temperature dependent X-ray powder pattern of **5a,** transforming to **5b** and **5c,** collected with Mo-$K_{\alpha1}$ radiation.

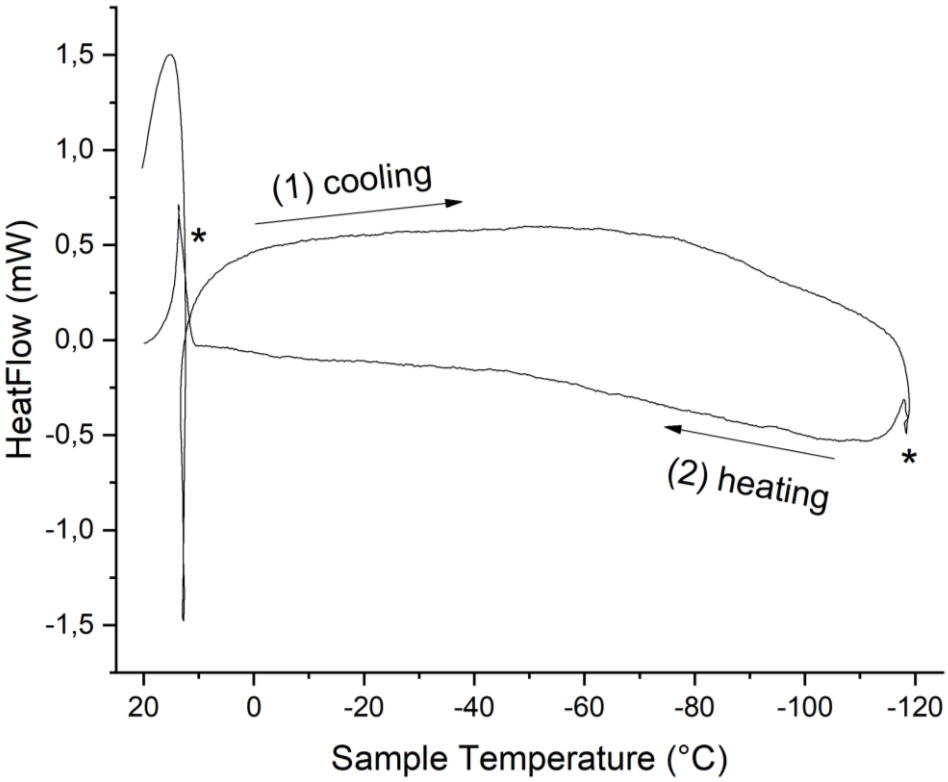

Figure S41. DSC-curve of $[MnBr_2(4\text{-}CNpy)_2]_n$ (**β-1a**): (1) Cooling from room temperature to -120°C, then (2) heating back to room temperature. Instrumental artefacts are marked by stars.

Table S1 Results of DTA/TG measurements of $[MX_2(4\text{-CNpy})_2]_n$. DTA peak temperatures, m_0: weight of starting compound, Δm_{exp}: relative experimental weight loss, experimental $\Delta m_{exp}/m_0$, calculated $\Delta m_{cal}/m_0$.

Compound	**T [°C]**	**m_0 [mg]**	**Δm_{exp} [mg]**	**$\Delta m_{exp}/m_0$ [%]**	**$\Delta m_{cal}/m_0$ [%]**
β-$[MnBr_2(4\text{-CNpy})_2]_n$ (**β-1a**)		22.328	0	0	0
$[MnBr_2(4\text{-CNpy})_1]_n$ (**1b**)	260.68		5.074	23.51	24.61
$[MnBr_2(4\text{-CNpy})_{1/2}]_n$ (**1c**)	328.38		2.624	15.89	16.32
$MnBr_2$	366.47		2.499	18.00	19.51
$[FeCl_2(4\text{-CNpy})_2]_n$ (**2a**)		21.506	0	0	0
$[FeCl_2(4\text{-CNpy})_1]_n$ (**2b**)	248.51		6.382	29.68	31.07
$[FeCl_2(4\text{-CNpy})_{1/3}]_n$ (**2c**)	347.61		4.294	28.39	30.06
$FeCl_2$	418.84		1.519	14.02	21.49
$[FeBr_2(4\text{-CNpy})_2]_n$ (**3a**)		22.000	0	0	0
$[FeBr_2(4\text{-CNpy})_1]_n$ (**3b**)	242.24		4.652	23.14	24.56
$[FeBr_2(4\text{-CNpy})_{1/3}]_n$ (**3c**)			3.422	19.73	21.70
$FeBr_2$ (→ $FeBr_3$)	355.22		1.003	7,20	13.86
$[CoCl_2(4\text{-CNpy})_2]_n$ (**4a**)		21.713	0	0	0
$[CoCl_2(4\text{-CNpy})_1]_n$ (**4b**)	251.96		6.342	29.21	30.80
$[CoCl_2(4\text{-CNpy})_{1/3}]_n$ (**4c**)	338.02		4.263	27.73	29.66
$CoCl_2$	409.70		2.050	18.45	21.08
$[CoBr_2(4\text{-CNpy})_2]_n$ (**5a**)		29.84	0	0	0
$[CoBr_2(4\text{-CNpy})_1]_n$ (**5b**)	252.08		7.023	23.54	30.80
$[CoBr_2(4\text{-CNpy})_{1/3}]_n$ (**5c**)	358.48		4.614	20.22	21.49
$CoBr_2$	389.72		2.231	12.25	13.69
$[CuBr_2(4\text{-CNpy})_2]$ (**6**)		6.119	0	0	0
$CuBr_2$ (→ CuBr)	252.54		2.405	60.69	48.24
α-$[ZnBr_2(4\text{-CNpy})_2]$ (**α-7**)		31.043	0	0	0
$ZnBr_2$	242.08		7.123	48.03	22.94
β-$[ZnBr_2(4\text{-CNpy})_2]$ (**β-7**)		13.56	0	0	0
$ZnBr_2$	236.71		3.039	48.03	25.89

Table S2-Part 1. Crystallographic data of $[MX_2(4\text{-CNpy})_2]_n$ (**1a**-**5a**).

	β -1a	**γ-1a**	**2a**	**3a**	**4a-PD**	**4a-SC**	**5a**
Compound	β-$[MnBr_2(4\text{-CNpy})_2]_n$	γ-$[MnBr_2(4\text{-CNpy})_2]_n$	$[FeCl_2(4\text{-CNpy})_2]_n$	$[FeBr_2(4\text{-CNpy})_2]_n$	$[CoCl_2(4\text{-CNpy})_2]_n$	$[CoCl_2(4\text{-CNpy})_2]_n$	$[CoBr_2(4\text{-CNpy})_2]_n$
CCDC number/ CSD code	1956119	1956120	1956117	1956115	1956112	UTIHIP	LATJOI
Structure determined from	Powder data	Powder data	Powder data	Powder data	Powder data	Single crystal data	Powder data
Formula	$C_{12}H_8Br_2MnN_4$	$C_{12}H_8Br_2MnN_4$	$C_{12}H_8Cl_2FeN_4$	$C_{12}H_8Br_2FeN_4$	$C_{12}H_8Cl_2CoN_4$	$C_{12}H_8Cl_2CoN_4$	$C_{12}H_8Br_2CoN_4$
MW /g·mol^{-1}	422.96	422.96	334.97	423.87	338.06	338.06	426.96
Crystal system	Monoclinic	Orthorhombic	Monoclinic	Orthorhombic	Monoclinic	Monoclinic	Orthorhombic
Space group (No.)	*P* $2_1/n$ (14)	*P nnm* (58)	*P* $2_1/n$ (14)	*P nnm* (58)	*P* $2_1/c$ (14)	*P* $2_1/c$ (14)	*P nnm* (58)
***a* /Å**	27.0744(7)	27.1046(6)	26.5605(10)	26.9168(11)	3.628870(42)	3.608(2)	26.8461(15)
***b* /Å**	7.38192(18)	7.4288(3)	7.1868(2)	7.3429(2)	7.15642(12)	7.065(5)	7.31908(32)
***c* /Å**	3.83783(11)	3.86070(12)	3.66280(7)	3.79547(10)	26.46185(42)	26.342(4)	3.77080(11)
***α* /°**	90	90	90	90	90	90	90
***ß* /°**	91.182(3)	90	95.365(3)	90	93.3930(16)	92.093(6)	90
***γ* /°**	90	90	90	90	90	90	90
***V* /Å^3**	766.87(4)	777.37(4)	696.11(4)	750.17(4)	686.002(18)	671.0(6)	740.920
Z, Z'	2, ½	2, ¼	2, ½	2, ¼	2, ½	2, ½	2, ¼
Site symmetry of M	$\bar{1}$	$\bar{1}$	$\bar{1}$	$\bar{1}$	$\bar{1}$	$\bar{1}$	$\bar{1}$
T /K	298	478	298	298	298	293	298
Radiation type	Cu $K\alpha_1$	Cu $K\alpha_1$	Cu $K\alpha_1$	Cu $K\alpha_1$	Mo $K\alpha_1$	Mo $K\alpha$	Mo $K\alpha_1$
Wavelength /Å	1.54056	1.54056	1.54056	1.54056	0.70930	0.71073	0.70930
$2\Theta_{min}$ /°	3	3	3	3	1.6150	-	1
$2\Theta_{max}$ /°	100	100	90	80	89.9046	-	60
psd step in 2Θ /°	0.09	0.09	0.09	0.09	0.125	-	0.09
time/step /sec	120	80	160	130	30	-	180
number of scans	2	2	1	1	2	-	3
***R_p* /%**	2.044	2.304	1.118	1.801	3.634	-	1.389
***R_{wp}* /%**	2.915	2.914	1.465	2.374	4.834	-	1.891
***R_{exp}* /%**	1.976	2.820	1.123	1.632	3.562	-	1.783
GOF	1.476	1.033	1.305	1.455	1.357	1.172	1.060
***R_p'* /% [a]**	18.774	11.862	24.007	20.053	9.249	-	17.81
***R_{wp}'* /% [a]**	15.827	28.219	17.657	15.685	10.106	-	13.06
***R_{exp}'* /% [a]**	10.726	18.035	13.535	10.782	7.446	-	12.32

a) R_p', R_{wp}' and R_{exp}' values are background corrected according to the reference [38].

Table S2-Part 2. Crystallographic data of $[MBr_2(4\text{-}CNpy)_2]_{(n)}$ (**6, α-7, β-7**).

	6	**α-7**	**β-7**
Compound	$[CuBr_2(4\text{-}CNpy)_2]_n$	α-$[ZnBr_2(4\text{-}CNpy)_2]$	β-$[ZnBr_2(4\text{-}CNpy)_2]$
CCDC number/ CSD code	1956113	1956121	1956122
Structure determined from	Powder data	Powder data	Powder data
Formula	$C_{12}H_8Br_2CuN_4$	$C_{12}H_8Br_2ZnN_4$	$C_{12}H_8Cl_2ZnN_4$
MW /g·mol^{-1}	431.57	433.41	433.41
Crystal system	Monoclinic	Monoclinic	Monoclinic
Space group (No.)	*P* $2_1/n$ (14)	*C* 2/*c* (15)	*P* $2_1/c$ (14)
***a* /Å**	7.30106(14)	28.4031(3)	16.0185(4)
***b* /Å**	25.8712(6)	7.73326(8)	12.09069(19)
***c* /Å**	3.98420(7)	17.2427(2)	7.89902(13)
***α* /°**	90	90	90
***ß* /°**	97.3176(13)	126.9230(6)	94.8775(12)
***γ* /°**	90	90	90
***V* /Å^3**	746.44(3)	3027.76(6)	1524.30(5)
Z, Z'	2, ½	8, 1	4, 1
Site symmetry of M	$\bar{1}$	1	1
T /K	298	298	298
Radiation type	Cu $K\alpha_1$	Cu $K\alpha_1$	Cu $K\alpha_1$
Wavelength /Å	1.54056	1.54056	1.54056
$2\Theta_{min}$ /°	3	3	3
$2\Theta_{max}$ /°	80	80	80
psd step in 2Θ /°	0.09	0.09	0.09
time/step / sec	150	150	120
number of scans	1	1	1
R_p /%	2.681	3.380	3.239
R_{wp} /%	3.699	4.356	4.213
R_{exp} /%	2.904	3.642	3.452
GOF	1.274	1.196	1.220
R_p' /% [a]	5.762	7.676	6.397
R_{wp}' /% [a]	7.355	8.016	7.149
R_{exp}' /% [a]	5.775	6.703	5.858

Table S3. Crystallographic data of $[MX_2(4\text{-CNpy})_1]_n$ (**1b-5b**).

	1b	**2b**	**3b**	**4b**	**5b**
Compound	$[MnBr_2(4\text{-CNpy})_1]_n$	$[FeCl_2(4\text{-CNpy})_1]_n$	$[FeBr_2(4\text{-CNpy})_1]_n$	$[CoCl_2(4\text{-CNpy})_1]_n$	$[CoBr_2(4\text{-CNpy})_1]_n$
CCDC number/ CSD code	1956118	1956116	1956114	1956126	1956111
Structure determined from	Powder data	Powder data	Powder data	Powder data	Powder data
Formula	$C_6H_4Br_2MnN_2$	$C_6H_4Cl_2FeN_2$	$C_6H_4Br_2FeN_2$	$C_6H_4Cl_2CoN_2$	$C_6H_4Br_2CoN_2$
MW /g·mol^{-1}	318.85	230.86	319.76	233.95	322.85
Crystal system	Monoclinic	Monoclinic	Monoclinic	Monoclinic	Monoclinic
Space group (No.)	*P* 2/*m* (10)	*P m* (6)	*P* 2/*m* (10)	*P m* (6)	*P* 2/*m* (10)
***a* /Å**	12.4448(6)	7.6656(8)	12.4397(9)	7.7426(4)	12.4692(10)
***b* /Å**	3.82332(12)	3.57945(15)	3.75800(17)	3.57685(7)	3.76053(17)
***c* /Å**	9.8744(5)	7.7986(10)	9.6919(7)	7.6901(4)	9.6232(7)
***α* /°**	90	90	90	90	90
***ß* /°**	90.569(8)	102.157	90.459(8)	102.664(2)	89.870(15)
***γ* /°**	90	90	90	90	90
***V* /Å^3**	469.81(4)	209.18(4)	453.07(5)	207.790(16)	451.24(5)
Z, Z'	2, ½	1, ½	2, ½	1, ½	2, ½
Site symmetry of M	*m*	*m*	*m*	*m*	*m*
T /K	298	298	298	523	523
Radiation type	Cu $K\alpha_1$	Cu $K\alpha_1$	Cu $K\alpha_1$	Mo $K\alpha_1$	Mo $K\alpha_1$
Wavelength /Å	1.54056	1.54056	1.54056	0.70930	0.70930
$2\Theta_{min}$ /°	3	3	3	1	1
$2\Theta_{max}$ /°	90	90	80	50.26	50.26
psd step in 2Θ /°	0.09	0.09	0.09	0.125	0.125
time/step /sec	160	60	130	120	120
number of scans	1	1	1	2	2
***R_p* /%**	1.757	1.304	1.524	3.882	1.480
***R_{wp}* /%**	2.331	1.681	1.974	5.477	1.984
***R_{exp}* /%**	1.442	1.575	1.664	2.995	1.404
GOF	1.616	1.067	1.186	1.829	1.413
***R_p'* /% [a]**	18.116	40.719	27.077	10.365	19.766
***R_{wp}'* /% [a]**	14.684	23.746	18.263	11.476	14.496
***R_{exp}'* /% [a]**	9.087	22.252	15.403	6.274	10.260

Table S4. R-Values of the Rietveld refinements of $[MCl_2(4\text{-}CNpy)_1]_n$ (**2b, 4b**) in *P* 2/*m* using models with and without disorder.

	$[FeCl_2(4\text{-}CNpy)_1]_n$ (2b)		**$[CoCl_2(4\text{-}CNpy)_1]_n$ (4b)**	
	without disorder model	with disorder model	without disorder model	with disorder model
R_{bragg}	0.7160	0.5962	2.2730	3.2948
R_p /%	1.304	1.298	3.882	4.323
R_{wp} /%	1.681	1.673	5.477	5.749
R_{exp} /%	1.575	1.575	2.995	2.995
GOF	1.067	1.062	1.829	1.920
R_p' /% [a]	40.719	40.641	10.365	11.591
R_{wp}' /% [a]	23.746	23.665	5.477	12.063
R_{exp}' /% [a]	22.252	22.278	6.274	6.283

Table S5. Results of the Rietveld refinements of $[MBr_2(4\text{-}CNpy)_1]_n$ (**1b, 3b, 5b**) in space group *Pmma* without using the disorder-model.

	$[MnBr_2(4\text{-}CNpy)_1]_n$ (1b)	**$[FeBr_2(4\text{-}CNpy)_1]_n$ (3b)**	**$[CoBr_2(4\text{-}CNpy)_1]_n$ (5b)**
R_{bragg}	1.649	1.853	2.473
R_p /%	2.108	3.882	1.727
R_{wp} /%	2.951	3.023	2.484
R_{exp} /%	1.443	1.665	1.407
GOF	2.044	1.815	1.765
R_p' /% [a]	22.087	39.659	24.165
R_{wp}' /% [a]	18.629	28.939	18.214
R_{exp}' /% [a]	9.112	15.943	10.318

Table S6. Restraints applied for the 4-CNpy fragment in the Rietveld refinements.

Type of bond angle	**Angle [°]**	**Type of bond length**	**Length [Å]**
C=C-H	120	N=C	1.34
C=C=C	120	C=C	1.38
C-C≡N	180	C≡N	1.14
N=C=C	120	C-H	0.99
N=C-H	120	C-C	1.44

Table S7. Measurement protocol of the high temperature series to prepare $[CoCl_2(4\text{-}CNpy)_1]_n$ (**4b**) and $[CoBr_2(4\text{-}CNpy)_1]_n$ (**5b**) on the X-ray powder diffractometer.

Elapsed time [min]	**Step No.**	**Mode**	**Target temperature [°C]**	**Holding time before next step or measurement [min]**	**Measurement No.**
00:00	1	Ramp	40.0	0	
00:01	2	Ramp	90.0	0	
00:12	3	Hold	90.0	10	
00:13	4	Ramp	140.0	0	
00:23	5	Hold	140.0	10	
00:24	6	Ramp	190.0	0	
00:35	7	Hold	190.0	10	
00:36	8	Ramp	240.0	0	
00:47	9	Hold	240.0	10	
00:47	10	Ramp	250.0	0	
02:58	11	Hold	250.0	10	1
05:09	12	Hold	250.0	10	2

Table S8. Measurement protocol of the temperature series to monitor the phase transition of **β-1a** to **γ-1a** on the powder diffractometer.

Elapsed time [min]	Step No.	Mode	Target temperature [°C]	Holding time before next step or measurement [min]	Measurement No.
00:00	1	Ramp	20.0	0	
01:38	2	Hold	20.0	0	1
01:36	3	Ramp	22.0	0	
03:12	4	Hold	22.0	0	2
03:09	5	Ramp	24.0	0	
04:45	6	Hold	24.0	0	3
04:43	7	Ramp	26.0	0	
06:19	8	Hold	26.0	0	4
06:16	9	Ramp	28.0	0	
07:53	10	Hold	28.0	0	5
07:50	11	Ramp	30.0	0	
09:26	12	Hold	30.0	0	6
09:24	13	Ramp	32.0	0	
11:00	14	Hold	32.0	0	7
10:57	15	Ramp	30.0	0	
12:34	16	Hold	30.0	0	8
12:31	17	Ramp	28.0	0	
14:08	18	Hold	28.0	0	9
14:05	19	Ramp	26.0	0	
15:42	20	Hold	26.0	0	10
15:39	21	Ramp	24.0	0	
17:16	22	Hold	24.0	0	11
17:13	23	Ramp	22.0	0	
18:50	24	Hold	22.0	0	12
18:47	25	Ramp	20.0	0	
20:23	26	Hold	20.0	0	13

Text S1

Details on syntheses of $[MX_2(4\text{-}CNpy)_2]_{(n)}$ (1a-5a, 6, 7)

Synthesis of $[MnBr_2(4\text{-}CNpy)_2]_n$ (1a). $MnBr_2$ (1.0 g, 4.66 mmol) was dissolved in 15mL ethanol, 4-CNpy (0.97 g, 9.32 mmol) was dissolved in 35 mL ethanol. No precipitate formed after having mixed the solutions. The mixture was place in a fridge (8°C), where a light pink powder formed within three days. IR -C≡N: 2242 cm^{-1}.

Synthesis of $[FeCl_2(4\text{-}CNpy)_2]_n$ (2a). $FeCl_2 \cdot 6\ H_2O$ (0.5 g, 3.944 mmol) was dissolved in 70mL ethanol, 4-CNpy (1.64 g, 15.77 mmol) was dissolved in 80 mL ethanol. By mixing both solutions, an orange precipitate formed. IR -C≡N: 2243 cm^{-1}.

Synthesis of $[FeBr_2(4\text{-}CNpy)_2]_n$ (3a). $FeBr_2 \cdot x\ H_2O$ (0.45g, 4,2 mmol) was dissolved in 70 mL ethanol, 4-CNpy (0.91 g, 8.72 mmol) was dissolved in 80 mL methanol. No precipitate formed after having mixed the solutions. The mixture was place in a fridge (8°C), where a dark orange powder formed within two days. IR -C≡N: 2243 cm^{-1}.

Synthesis of $[CoCl_2(4\text{-}CNpy)_2]_n$ (4a). $CoCl_2 \cdot 6\ H_2O$ (1,0 g, 4,21 mmol) was dissolved in 10 mL methanol, 4-CNpy (0.44 g, 4.4 mmol) was dissolved in 10 mL methanol. By mixing both solutions, a lilac precipitate formed. IR -C≡N: 2241 cm^{-1}.

Synthesis of $[CoBr_2(4\text{-}CNpy)_2]_n$ (5a). $CoBr_2$ (0,53 g, 2,4 mmol) was dissolved in 8 mL ethanol, 4-CNpy (0.55 g, 5.3 mmol) was dissolved in 5 mL ethanol. No precipitate formed after having mixed the solutions. The mixture was heated to 70°C and a violet powder was obtained within one minute. IR -C≡N: 2247 cm^{-1}.

Synthesis of $[CuBr_2(4\text{-}CNpy)_2]_n$ (6). $CuBr_2$ (0,5 g, 2,23 mmol) was dissolved in 40 mL methanol, 4-CNpy (0.93 g, 8.92 mmol) was dissolved in 20 mL methanol. By mixing both solutions, an neon green precipitate formed. IR -C≡N: 2243 cm^{-1}.

Synthesis of $[ZnBr_2(4\text{-}CNpy)_2]$ (α-7/ β-7). $ZnBr_2$ (0,46 g, 2,22 mmol) was dissolved in 40 mL ethanol, 4-CNpy (0.49 g, 4.66 mmol) was dissolved in 20 mL ethanol. The solutions were mixed and colorless precipitate formed with two minutes. IR -C≡N: 2243 cm^{-1}.

Text S2

Details on preparation of $[MX_2(4\text{-}CNpy)_1]_n$

Preparation of $[MnBr_2(4\text{-}CNpy)_1]_n$ (1b). 1b was prepared by thermal decomposition of $[MnBr_2(4\text{-}CNpy)_2]_n$ (**1a**) at 230°C in the DTA-TG device. A greyish powder was obtained. IR -C≡N: 2242 cm^{-1} but should be around 2280 cm^{-1}. $[MnBr_2(4\text{-}CNpy)_1]_n$ easily reacts with water and oxygen and, unfortunately, IR data may be incorrect.

Preparation of $[FeCl_2(4\text{-}CNpy)_1]_n$ (2b). 2b was prepared by thermal decomposition of $[FeCl_2(4\text{-}CNpy)_2]_n$ (**2a**) at 220°C in the DTA-TG device. A yellow powder was obtained. IR -C≡N: 2276 cm^{-1}.

Preparation of $[FeBr_2(4\text{-}CNpy)_1]_n$ (3b). 3b was prepared by thermal decomposition of $[FeBr_2(4\text{-}CNpy)_2]_n$ (**3a**) at 260°C in the DTA-TG device. A dark red powder was obtained. IR -C≡N: 2284 cm^{-1}.

Preparation of $[CoCl_2(4\text{-}CNpy)_1]_n$ (4b). 4b was prepared by thermal decomposition of $[CoCl_2(4\text{-}CNpy)_2]_n$ (**4a**) at 250°C on the x-ray powder diffractometer. No IR spectrum was measured, because the sample always was obtained *in-situ*.

Preparation of $[CoBr_2(4\text{-}CNpy)_1]_n$ (5b). 5b was prepared by thermal decomposition of $[CoCl_2(4\text{-}CNpy)_1]_n$ (**5a**) at 250°C on the x-ray powder diffractometer. No IR spectrum was measured, because the sample was obtained *in-situ*.

Text S3

Further details on structure solution and Rietveld refinements.

$[MnBr_2(4\text{-}CNpy)_2]_n$ (β-1a). The first 20 peaks were selected for indexing in DASH which resulted in a monoclinic unit cell with Z = 2. Structure solution was then carried out using simulated annealing with DASH. A starting molecular model was derived from the known crystal structure of $[MnBr_2(4\text{-}CNpy)_2]_n$. The molecular fragment was restricted to rotate around the Mn atom. The Mn atom was placed on the origin, the bromine atom was fixed on (x,z,1/2), 4-CNpy was fixed on (x,y,0).

$[MnBr_2(4\text{-}CNpy)_2]_n$ (γ-1a). The first 20 peaks were selected for indexing in DASH which resulted in an orthorhombic unit cell with Z = 2. Structure solution was then carried out using simulated annealing with DASH. A starting molecular model was

derived from the known crystal structure of β-$[MnBr_2(4\text{-}CNpy)_2]_n$. The molecular fragment was restricted to rotate around the Mn-atom, Mn-atom and 4-cyanopyridine were fixed on a special position (0,0,0) during the simulated annealing.

$[MnBr_2(4\text{-}CNpy)_1]_n$ (1b). The structure is isotypic to $[NiBr_2(4\text{-}CNpy)_1]_n$. A Pawley fit was performed in TOPAS using the lattice parameters of $[NiBr_2(4\text{-}CNpy)_1]_n$ as starting values. First, background and instrumental parameters (zero point, axial divergence) were refined. Next, size and strain parameters were refined. Structure solution was then carried out with the simulated annealing algorithm of DASH using a starting molecular model derived from $[NiBr_2(4\text{-}CNpy)_1]_n$. The molecular fragment was restricted to rotate around the Mn atom, Mn atom and 4-cyanopyridine were fixed on a special position (0,0,0) during the simulated annealing. The Rietveld refinement was carried out with TOPAS. The Mn atom was placed on the origin, the bromine atom was fixed on (x,-1/2,z), the 4-cyanopyridine was fixed on (x,0,z).

$[FeCl_2(4\text{-}CNpy)_2]_n$ (2a). The first 20 peaks were selected for indexing in CONOGRAPH which resulted in a monoclinic unit cell with Z = 2. First, background and instrumental parameters (zero point, axial divergence) were refined. Next, size and strain parameters were refined. Structure solution was then carried out using simulated annealing in DASH. The molecular fragment ($FeCl_2(4cypy)_1$) was restricted to rotate around the Fe atom on special position (0,0,0). Rietveld refinement was carried out with TOPAS.

$[FeCl_2(4\text{-}CNpy)_1]_n$ (2b). $[FeCl_2(4\text{-}CNpy)_1]_n$ is isotypic to $[NiCl_2(4\text{-}CNpy)_1]_n$. At first, a Pawley fit was performed in TOPAS refining background and instrumental parameters (zero point, axial divergence). Next, size and strain parameters were refined. The crystal structure of $[NiCl_2(4\text{-}CNpy)_1]_n$ was used as starting point for the subsequent structure refinement. The Rietveld refinement was carried out with TOPAS.

$[FeBr_2(4\text{-}CNpy)_2]_n$ (3a). The first 20 peaks were selected for indexing in CONOGRAPH and DASH, which both resulted in a orthorhombic unit cell with Z = 2. Structure solution was then carried out using simulated annealing with DASH. A starting molecular model was derived from the known crystal structure of $[NiBr_2(4\text{-}CNpy)_2]_n$. The Fe atom was placed on the origin, the bromine atom was fixed on (x,z,1/2), the 4-cyanopyridine was restrained flat in the mirror plane. The Rietveld refinement was carried out with TOPAS.

[$FeBr_2$(4-CNpy)$_1$]$_n$ (3b). The structure is isotypic to [$NiBr_2$(4-CNpy)$_1$]$_n$ and [$MnBr_2$(4-CNpy)$_1$]$_n$. A Pawley fit was performed in TOPAS (Coelho, 2018) using the lattice paramters of [$MnBr_2$(4-CNpy)$_1$]$_n$ as starting values. First, background and instrumental parameters (zero point, axial divergence) were refined. Next, size and strain parameters were refined. Structure solution was then carried out with the simulated annealing algorithm of DASH using a starting molecular model derived from [$NiBr_2$(4-CNpy)$_1$]$_n$. The molecular fragment was restricted to rotate around the Fe-atom. The Fe atom was placed on the origin, the bromine atom was fixed on (x,-1/2,z), the 4-cyanopyridine was fixed on (x,0,z). The Rietveld refinement was carried out with TOPAS.

[$CoCl_2$(4-CNpy)$_2$]$_n$ (4a). The structure of [$CoCl_2$(4-CNpy)$_2$]$_n$ was determined from single crystal data (UTIHIP) by Chen et. al in 2011. A Pawley fit was performed in TOPAS using these lattice parameters as starting values. First, background and instrumental parameters (zero point, axial divergence) were refined. Next, size and strain parameters were refined. Structure solution was then carried out with the simulated annealing algorithm of DASH using one Co and one Cl atom, and one 4cypy ring as fragments. The Co atom was placed on special position (0,0,0). Rietveld refinement was carried out with TOPAS (Coelho, 2018).

[$CoCl_2$(4-CNpy)$_1$]$_n$ (4b). The compound is isotypic to [NiCl2(4cypy)1]n and [FeCl2(4cypy)1]n. A Pawley fit was performed in TOPAS (Coelho, 2018) using the lattice parameters of the isotypic Ni-compound. First background and instrumental parameters (zero point, axial divergence) were refined. Next, size and strain parameters were refined. Structure solution was then carried out with the simulated annealing algorithm of DASH using one Co atom, two Cl atoms and one 4cypy ring as fragments. The Co atom was placed on special position (0,0,0), the pyridine ring was placed on (x,0,z) and the Cl atoms were placed on (x,1/2,z). Rietveld refinement was carried out with TOPAS.

[$CoBr_2$(4-CNpy)$_1$]$_n$ (5b). The structure is isotypic to [$MnBr_2$(4-CNpy)$_1$]$_n$, [$FeBr_2$(4-CNpy)$_1$]$_n$ and [$NiBr_2$(4-CNpy)$_1$]$_n$. A Pawley fit was performed in TOPAS (Coelho, 2018) using the lattice parameters of [$NiBr_2$(4-CNpy)$_1$]$_n$ as starting values. First, background and instrumental parameters (zero point, axial divergence) were refined. Next, size and strain parameters were refined. Structure solution was then carried out with the simulated annealing algorithm of DASH using one Co atom, two Br atoms

and one 4-cypy as fragments. The Co atom was placed on the origin, the bromine atom was fixed on (x,-1/2,z), the 4-cyanopyridine was fixed on (x,0,z).

$[CuBr_2(4\text{-}CNpy)_2]_n$ (6). At first, a Pawley fit was performed in TOPAS to refine background and instrumental parameters (zero point, axial divergence). Next, size and strain parameters were refined. The crystal structure of $[CuCl_2(4\text{-}CNpy)_2]_n$ was used as starting point for the subsequent structure refinement. Rietveld refinement was carried out with TOPAS.

$[ZnBr_2(4\text{-}CNpy)_2]_n$ (α-7). The first 20 peaks were selected for indexing in CONOGRAPH and DASH which resulted unanimously in a monoclinic unit cell with Z = 8. First, background and instrumental parameters (zero point, axial divergence) were refined. Next, size and strain parameters were refined. Structure solution was then carried out using simulated annealing with DASH. A starting molecular model was derived from the crystal structure of $[ZnBr_2(4\text{-}CNpy)_2]$. The molecular fragment was restricted to rotate around the Zn atom during the simulated annealing procedure. Rietveld refinement was carried out with TOPAS.

$[ZnBr_2(4\text{-}CNpy)_2]_n$ (β-7). The first 20 peaks were selected for indexing in CONOGRAPH which resulted in a monoclinic unit cell with Z = 4. First, background and instrumental parameters (zero point, axial divergence) were refined. Next, size and strain parameters were refined. Structure solution was then carried out using simulated annealing with DASH. The starting molecular model for the β-phase was derived from the crystal structure of α-$[ZnBr_2(4\text{-}CNpy)_2]$. The molecular fragment was restricted to rotate around the Zn atom during simulated annealing. Rietveld refinement was carried out with TOPAS.